Report

TWO-COLOR PHOTOCONDUCTIVE DETECTORS

James W. Reynolds

HONEYWELL
Radiation Center
2 Forbes Road
Lexington, Massachusetts 02173

August 13, 1971

Final Report

Prepared for

GODDARD SPACE FLIGHT CENTER
Greenbelt, Maryland 20771

1. Report No.	2. Government Accession No.	3. Recipient's Catalog No.
4. Title and Subtitle		5. Report Date
		6. Performing Organization Code
7. Author(s) James W. Reynolds		8. Performing Organization Report No.
9. Performing Organization Name and Address Honeywell Radiation Center 2 Forbes Road, Lexington, Mass. 02173		10. Work Unit No.
		11. Contract or Grant No. NASA 5-21150
12. Sponsoring Agency Name and Address		13. Type of Report and Period Covered Final 18 Sept. 1970 - March 1970 18 Dec. 1970 - March 1971
		14. Sponsoring Agency Code

15. Supplementary Notes

(See following page)

16. Abstract

17. Key Words	18. Distribution Statement

19. Security Classif. (of this report)	20. Security Classif. (of this page)	21. No. of Pages	22. Price
Unclassified	Unclassified	65	

ABSTRACT

This is the Final Technical Report for NASA/Goddard, Contract NAS 5-21150 for the development of two-color "sandwiched" photoconductive (Hg,Cd)Te detectors.

This two-color approach to the problem of multispectral detection uses a sandwich configuration in which two detectors of different cutoff wavelengths are superimposed and intimately coupled by an optical impedance matching layer. Advantages of this sandwich detector include the elimination of channel synchronization and time sharing. The final detectors are capable of very high spectral resolution at an operating temperature of 95 °K or higher.

Fabrication procedures have been developed for making high performance two-color detectors in array form. The bottom detector serves as the substrate for the top detector. An epoxy was developed having a high transmission bandpass at the peak wavelength response of the bottom detector, rejection of the 9.6 μm ozone emission band, high electrical isolation, and good mechanical properties. The bottom detector may show a higher spectral detectivity as the bottom element of a two-color detector than as a single-color detector because the top detector acts as a cold filter.

Honeywell has delivered to NASA/GSFC two detectors with the following characteristics:

Detector Y1: (95 °K)

Top Element:

D^*_λ (8.5 μm, 10 kHz, 1) = 3.52×10^9 $cmHz^{1/2}/watt$

$\lambda_{cutoff} \sim 8.8$ μm

Bottom Element:

D^*_λ (10.5 μm, 10 kHz, 1) = 9.58×10^9 $cmHz^{1/2}/watt$

$\lambda_{cutoff} \sim 11.1$ μm

$\lambda_{cut\text{-}on} \sim 9.8$ μm

Detector Y2: (95 °K)

Top Element:

D^*_λ (9 μm, 10 kHz, 1)=4.84 x 10^9 $cmHz^{1/2}$/watt

$\lambda_{cutoff} \sim 9.3$ μm

Bottom Element:

D^*_λ (10.5 μm, 10 kHz, 1)=1.12 x 10^9 $cmHz^{1/2}$/watt

$\lambda_{cutoff} \sim 11.7$ μm

$\lambda_{cut\text{-}on} \sim 10.2$ μm

All of the detector elements exceed the detectivity design goal by 50% except for the bottom element of Y2, which was down by less than 20% after the correction factor for the two windows is taken.

TABLE OF CONTENTS

LIST OF ILLUSTRATIONS

LIST OF ILLUSTRATIONS (CONT.)

SECTION I

INTRODUCTION

This is the Final Technical Report for NASA/Goddard Contract NAS 5-21150. The purpose of this program is to develop two-color "sandwiched" photoconductive mercury-cadmium-telluride far infrared detectors.

This two-color approach to the problem of multispectral detection uses a sandwich configuration in which two detectors of different cutoff wavelengths are superimposed and intimately coupled by an optical impedance matching layer. Advantages of this sandwich detector include the elimination of channel synchronization and time sharing. The final detectors are capable of very high spectral resolution at an operating temperature of 95 °K or higher.

The design goals for two detectors to be delivered at the completion of the contract are (using an external filter if necessary):

Specific peak detectivities $\geq 2 \times 10^9$ cmHz$^{1/2}$/watt

Top element half response points: 8.4 - 9.3 μm

Bottom element half response points: 10.2 - 11.4 μm

Nominal operating temperature $\geq$ 95 °K

Frequency: 10,000 Hz

The program was divided into five major areas of study:

1. A theoretical and experimental study to combine the elevated operating temperature model with optical multilayer theory resulting a two-color detector, computer-aided program.

2. Investigation of infrared transmitting epoxies and dielectric matching layers for adhesion, electrical isolation, stability, and optimum optical coupling.

3. Development of fabrication techniques which yield the desired final configuration and insure active area alignment.

4. Theoretical and experimental study of absorption edges and filtering requirements to attain narrow spectral bandwidths for high resolution.

5. Experimental investigations of temperature dependence and 1/f noise to attain high two-color detector performance above 95 °K.

The program plan for the program is shown in Figure 1. Honeywell has studied these five major areas with good success. During the program, Honeywell developed a high yield technology required to reproducibly fabricate reliable high performance two-color (Hg,Cd)Te detectors with high spectral resolution and rejection of the ozone emission band at 9.6 μm.

Honeywell has delivered to NASA/GSFC two detectors having the following characteristics:

Detector Y1: (95 °K)

Top Element:

D^*_λ (8.5 μm, 10 kHz, 1) = 3.52×10^9 $cmHz^{1/2}/watt$

$\lambda_{cutoff} \sim 8.8$ μm

Bottom Element:

D^*_λ (10.5 μm, 10 kHz, 1) = 9.58×10^9 $cmHz^{1/2}/watt$

$\lambda_{cutoff} \sim 11.1$ μm

$\lambda_{cut\text{-}on} \sim 9.6$ μm

Detector Y2: (95 °K)

Top Element:

D^*_λ (9 μm, 10 kHz, 1)=4.84×10^9 $cmHz^{1/2}/watt$

$\lambda_{cutoff} \sim 9.3$ μm

Bottom Element:

D^*_λ (10.5 μm, 10 kHz, 1) = 1.12×10^9 $cmHz^{1/2}/watt$

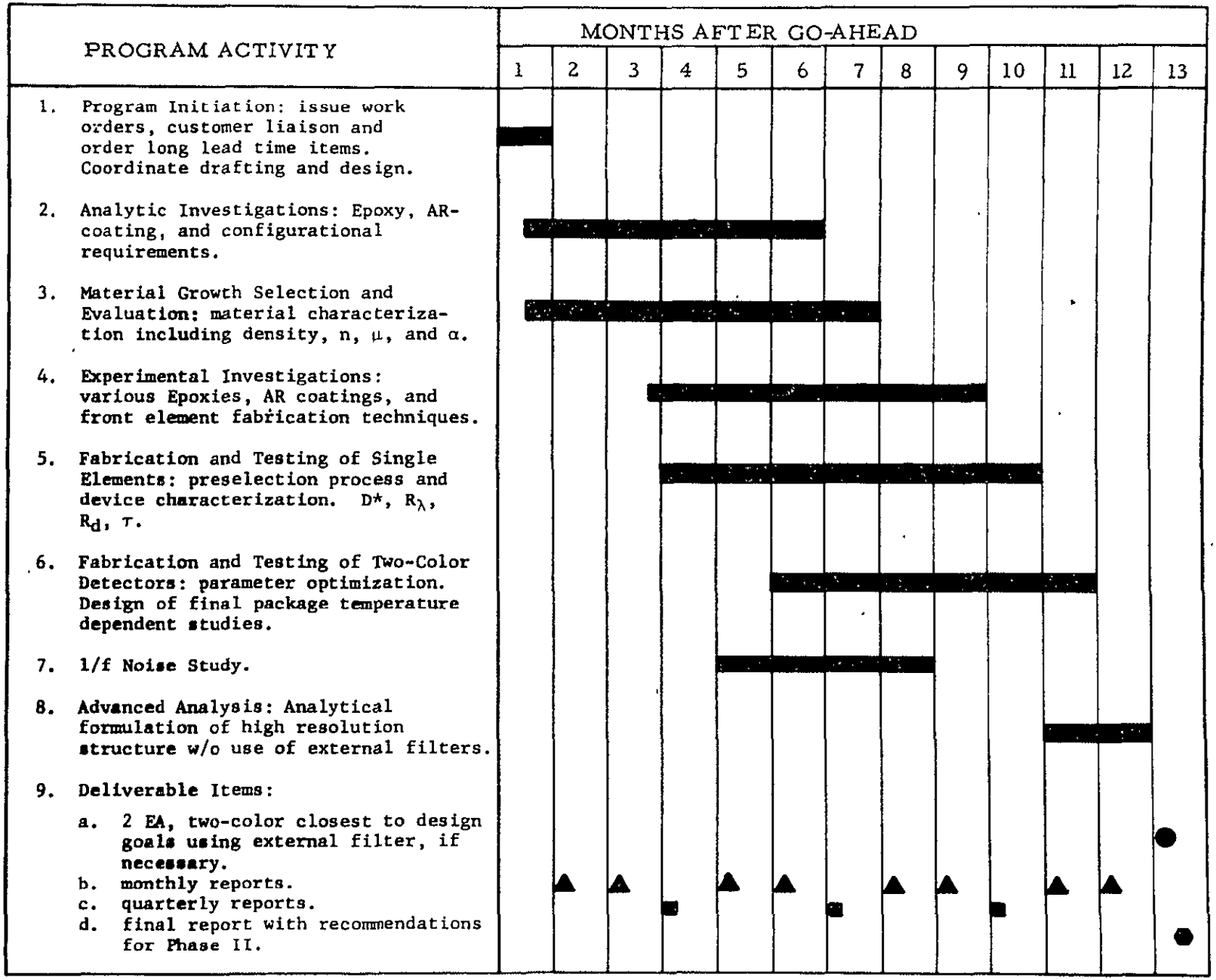

Figure 1. PROGRAM PLAN PHASE I - TWO-COLOR DETECTOR

$\lambda_{cutoff} \sim 11.7\ \mu m$

$\lambda_{cut\text{-}on} \sim 10.2\ \mu m$

All of the detector elements exceed the detectivity design goal by 50% except for the bottom element of Y2 which was down by less than 20% after the correction factor for the two windows is taken, as discussed in Section III.

Section II is a detailed discussion of two-color detector fabrication procedures and performance characteristics. Section III gives the performance of the two detectors delivered under the contract. Section IV contains recommendations for future work.

The major findings of the development program are:

1. Two-color detectors may be made in the parallel configuration without a substrate for the top detector in high yield.

2. The epoxy developed provides good mechanical, chemical, and optical properties, including rejection of the 9.6 μm ozone emission band.

3. The bottom detector may exhibit higher performance as the bottom element of a two-color detector than as a single-color detector due to the cold filtering of the top detector.

4. There appears to be no significant increase in 1/f noise for the bottom element of a two-color detector as compared to single element detectors.

5. Classical two-carrier photoconductivity theory describes two-color detectors, and the results are part of Honeywell's capability for the complete computer prediction of photodetector properties.

SECTION II

TECHNICAL DISCUSSION

2.1 TWO-COLOR DETECTOR DESIGN AND FABRICATION

2.1.1 Configurations and Design of Two-Color Detectors

A significant accomplishment of this two-color detector development program was the development of a configuration and design and procedures for fabrication of two-color (Hg,Cd)Te photodetectors. The optimum configuration is the parallel configuration shown in Figure 2a. This is the configuration for the two final detectors delivered to NASA/GSFC under this program. The major advantages of the parallel configuration are:

1. Ease of fabrication
2. Higher yield
3. Improved uniformity
4. High density array capability

In the parallel configuration, the top and bottom detectors are aligned parallel to one another so that the contacts of the top detector are directly above those of the bottom detector (see Figure 2a). The parallel configuration is characterized by the fact that the top detector has no substrate other than the bottom detector, thus eliminating transmission losses in the upper substrate and epoxy which is characteristic of the crossed configuration.

A second configuration for two-color detectors is the crossed configuration shown in Figure 2b. Two detectors are epoxied separately to Irtran II substrates with an infrared transmitting epoxy and then epoxied to one another in a crossed pattern. Two-color detectors fabricated during the first quarter of this contract were in this configuration. The crossed configuration is undesireable because it lends itself readily to problems of active area alignment and light leaks.

Further, the crossed configuration (1) results in reduced yield in fabrication, and (2) does not lend itself to making high density arrays.

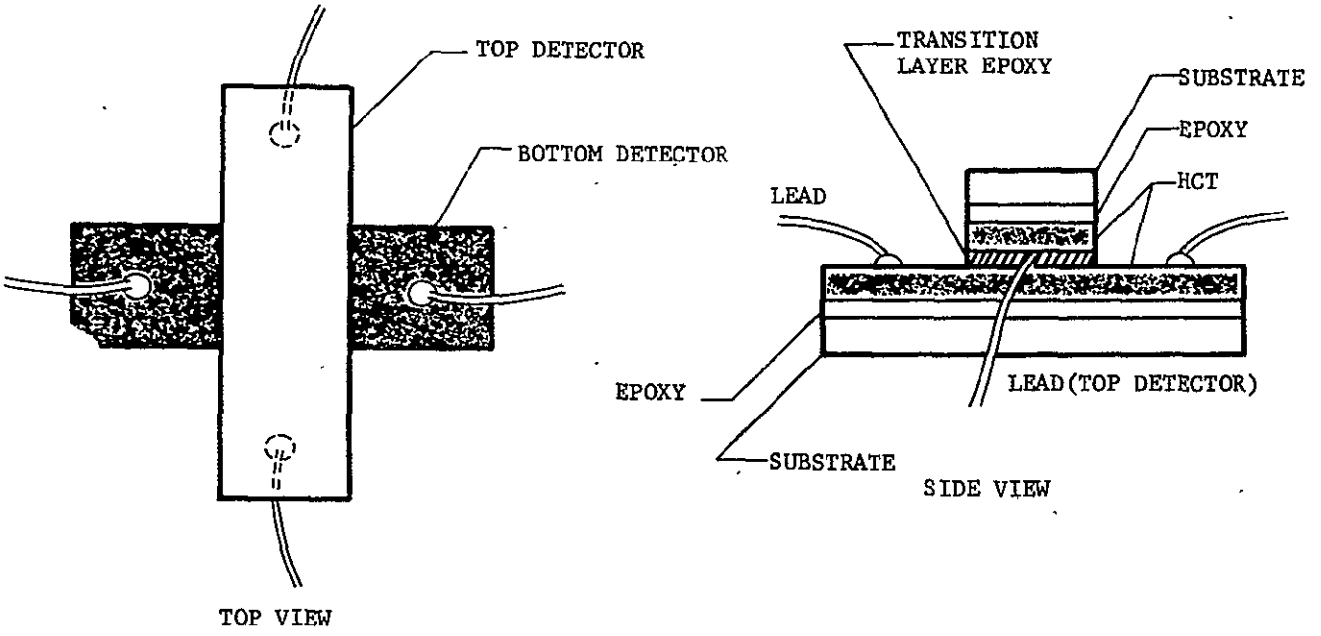

Figure 2a PARALLEL CONFIGURATION OF TWO DETECTORS

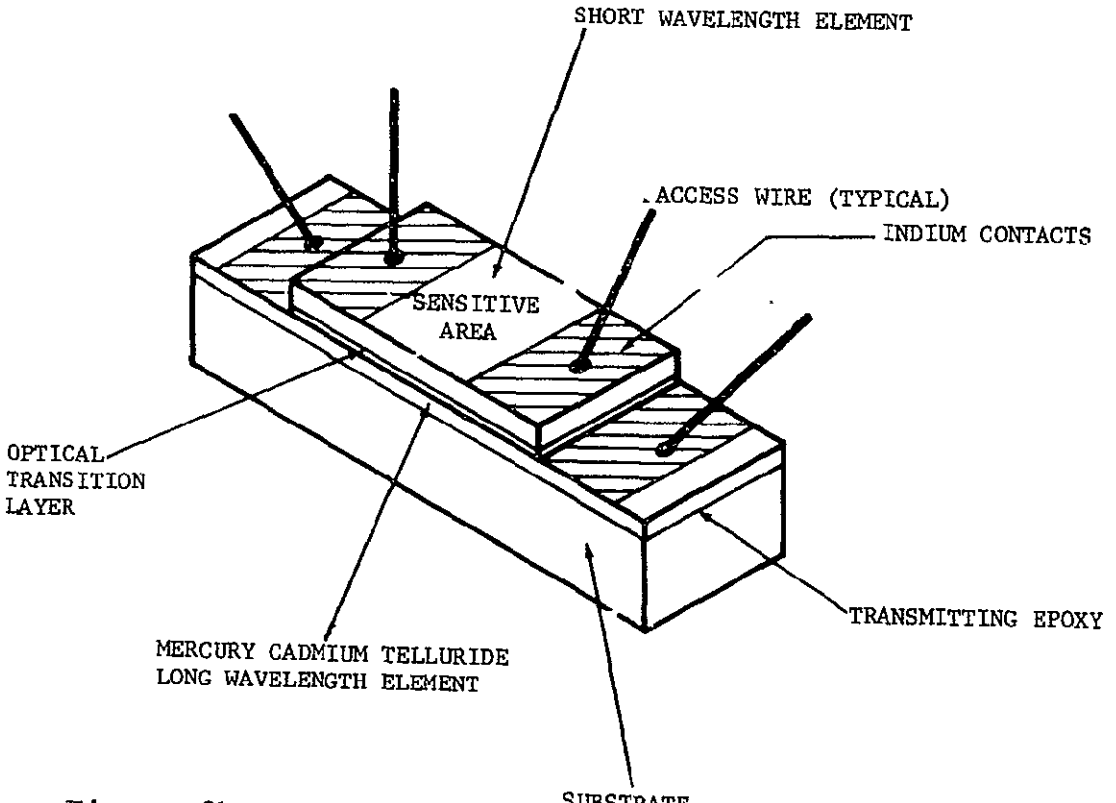

Figure 2b A CONFIGURATION FOR TWO-COLOR DETECTORS (CROSSED)

The essential features of the parallel design for two-color detectors are shown in a schematic drawing in Figure 3. First, the active areas of the top and bottom detectors are equal in area and optically aligned. Next, the thickness of the epoxy layer separating the top and bottom detectors is very thin (about 0.0005 inch) thereby minimizing transmission losses, to the bottom detector. The top detector is made to be slightly wider than the bottom detector, and this reduces short wavelength radiation leakage to the bottom detector. The substrate for the top detector is the bottom detector. Good mechanical properties occur without an additional substrate. This in turn reduces the optical losses.

In the above design the epoxy plays a most important role. First, good mechanical strength between the top and bottom detector is obtained thereby permitting fabrication of the top detector in high yield without cracking or breaking. Next, in the optical bandpass of the bottom detector (10.2-11.6 μm) the absorption coefficient of the epoxy is small (about 175 cm^{-1}) so that for epoxy thicknesses of 1.25×10^{-3} cm, little radiation absorption in the epoxy layer occurs. However, at certain wavelengths the epoxy shows strong absorption bands due to epoxy molecular bond stretching and bonding. At 9.6 μm this occurs, yielding ozone rejection. This was a design goal of the program. Finally, high electrical rejection results; electrical resistances between top and bottom detectors are typically 10 megohms. The spectral response of a typical two-color detector is shown in Figure 4.

2.1.2 Fabrication Procedures

The following procedure is employed for fabricating two-color detectors. A slab of material for the bottom detector elements is chosen in the usual way, using previously measured density resistivity and Hall mobility data. An array of elements are fabricated in the usual manner. The elements of the array are then tested for detectivity, spectral response, and resistance. Those detectors having acceptable detectivities and the proper peak and cutoff wavelengths are then separated from the other elements of the row. (Hg,Cd)Te grows uniformly in the horizontal direction; that is, in the direction from which the rows are cut so that generally eight or more consecutive elements of a row will have the required cutoff wavelengths. The exact number will depend upon the particular slab and on the wavelength tolerance.

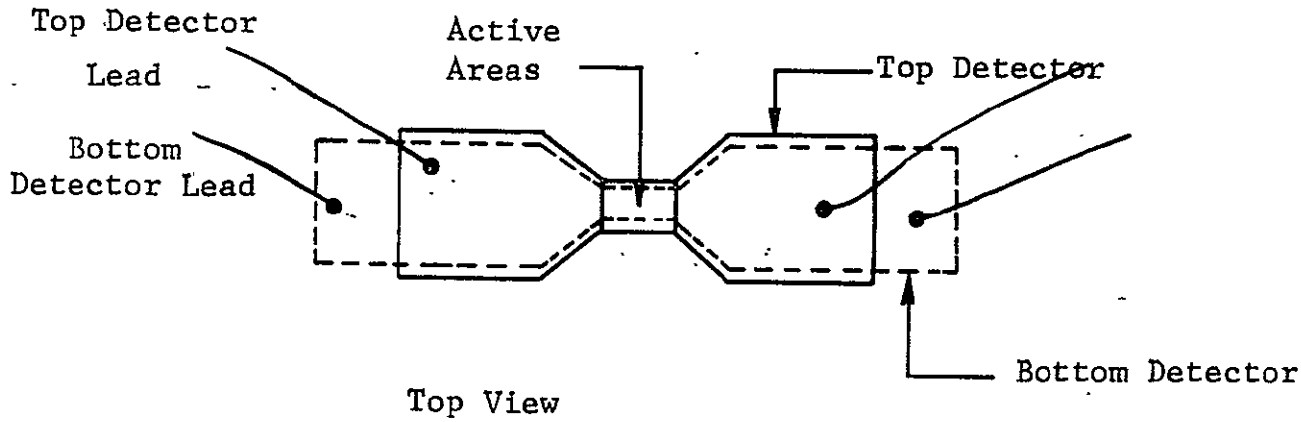

Top View

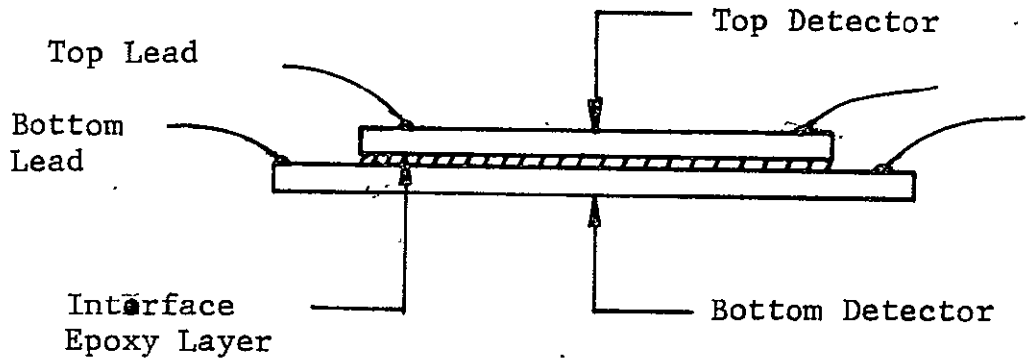

Side View

Figure 3 SCHEMATIC OF PARALLEL CONFIGURATION B

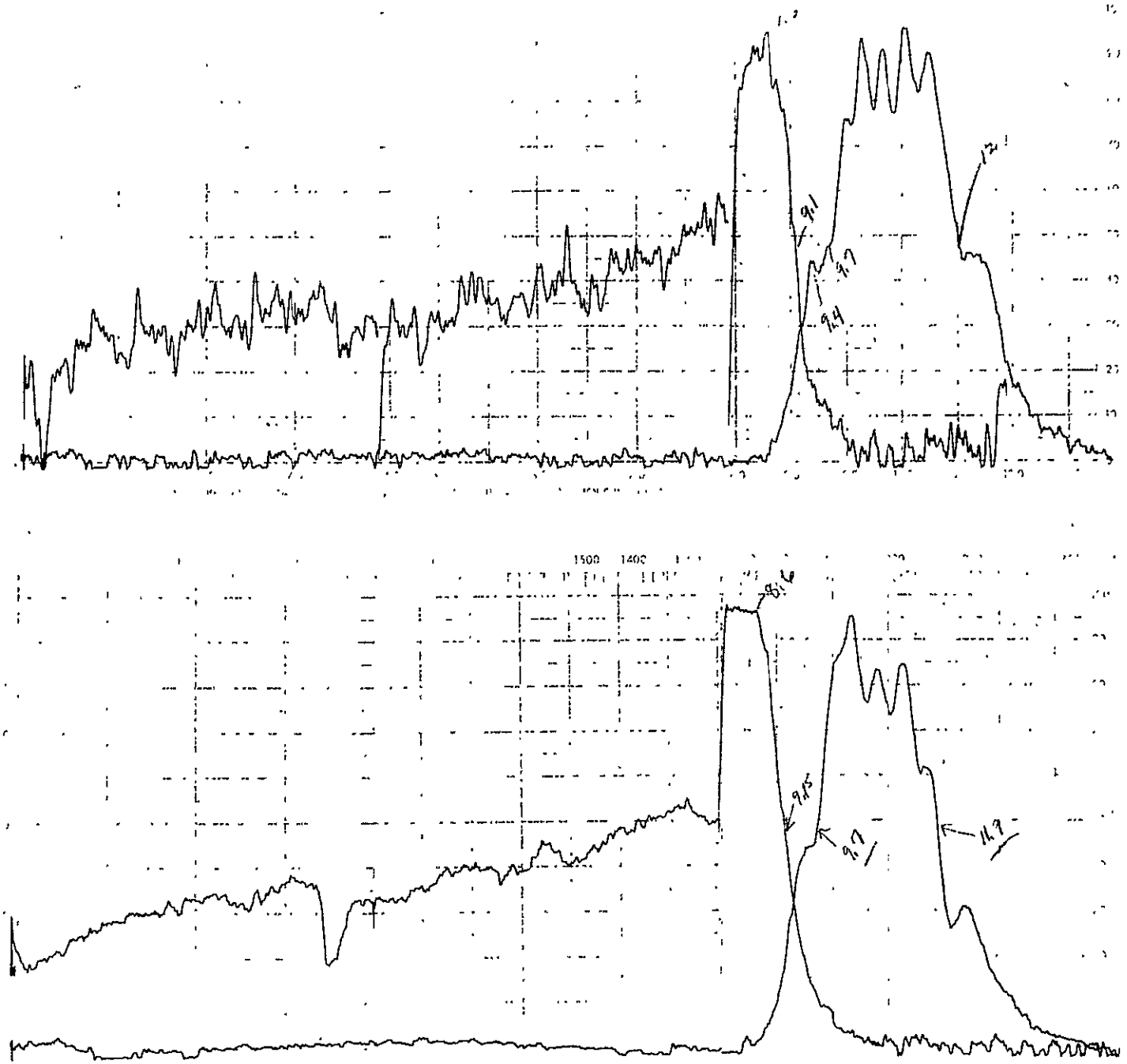

Figure 4 SPECTRAL RESPONSE OF TWO-COLOR (Hg,Cd)Te DETECTORS, SLAB 165/ROW 4 ON SLAB 190/ROW D.

Next, a slab of material is chosen for the top elements. The selection of material of the proper cutoff wavelength for the top element of a two-color detector represents a critical area for the fabrication of two-color elements when very high resolution is required. A nondestructive evaluation method was developed during the third quarter and has been used successfully for fabricating two-color detectors. The method utilizes the spectral response of the detector.

Like other alloys grown from the melt, $Hg_{1-x}Cd_xTe$ crystals vary in composition through the crystal. For most applications the composition may be determined adequately by density measurements. However, for the present program, the density approach does not give sufficient accuracy, and further is a destructive evaluation method.

Optical evaluation can provide a more accurate compositional determination in a nondestructive approach. Emphasis has been on the detector spectral response; however, in future programs we intend to use both optical absorption and spectral response to achieve highest resolution. Optical absorption is expected to be of greater importance for the fabrication of large arrays of n-color detectors at low cost.

The present procedure is to cut a slab of $Hg_{1-x}Cd_xTe$ into strips which are 0.030 inch wide and 0.030 thick. Then five contact pads are evaporated on each strip and lead wires are attached resulting in four large area detectors. The detectors are then measured for spectral response. Selected material of the proper cutoff wavelength is then used for the fabrication of detectors. (See Figure 5).

The contacts from the preliminary evaluation are removed by lapping. Then the material is ready for fabrication into top detectors.

The section of material for the top slab is then placed on the array of bottom detectors, using the detectors at each end of the bottom element array to align the elements and spacer bars to maintain proper separation. The net result is n-2 elements of two-color detectors, where n is the number of bottom detector elements.

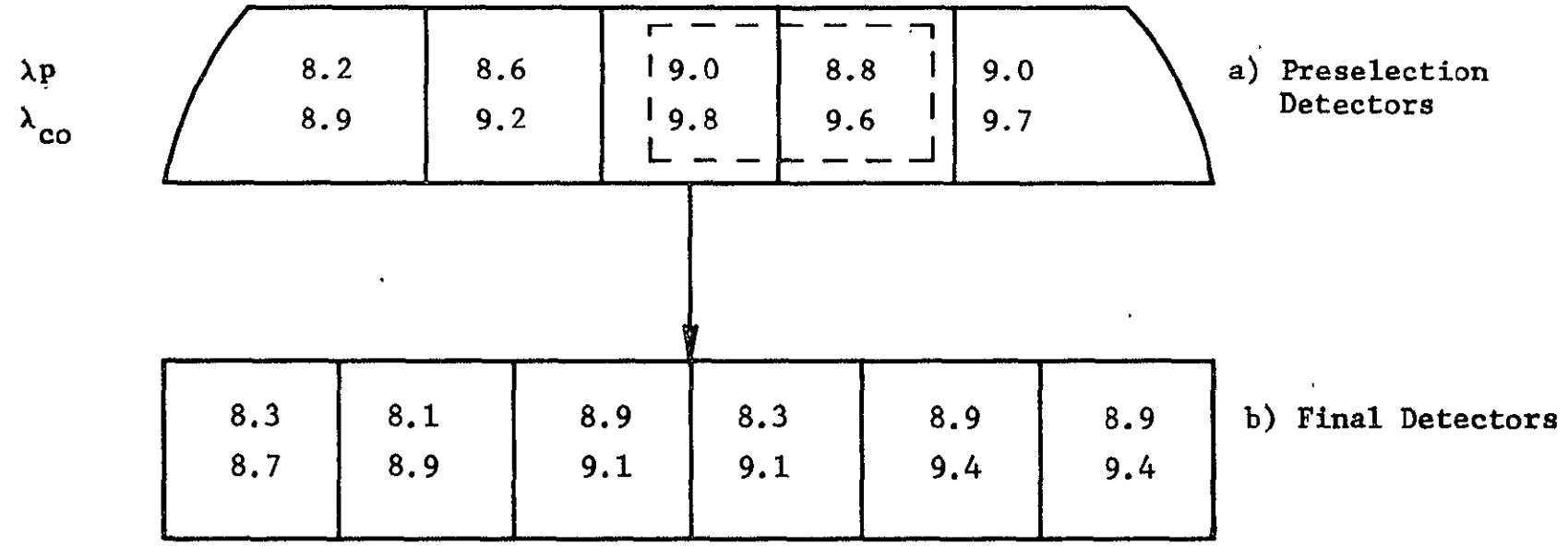

Figure 5 PEAK AND CUTOFF WAVELENGTHS OF PHOTOCONDUCTORS (a) PRESELECTION DETECTORS AND (b) TOP ELEMENTS AT 2-COLOR

Figure 6 shows the strip of material of the proper wavelength for the top detector mounted on fabricated bottom detectors. Figure 7 shows the completed two-color detector in the parallel configuration.

The above procedure was used to fabricate the array of six elements of two-color detectors discussed in Section 2.2.

There is a slight discrepancy between the values of the cutoff wavelength for the preliminary test detectors and the final two-color detectors. This result is due probably to the difference in thickness of the two detectors. The preliminary detectors were ~0.030 inch, whereas the thickness of the top detectors of the array was ~0.0015 inch. A similar discrepancy occured later when an absorption methods were used in an attempt to locate prime material.

2.1.3 Transition Layer Epoxies

Of prime importance in the development and fabrication of two-color detectors is the selection of a suitable transition layer which separates the top and bottom detectors. Ideally, the transition layer should consist of an infrared transmitting epoxy and appropriate antireflection films for dielectric matching. Requirements for an acceptable transition layer epoxy are:

1. High optical transmission in the spectral region of interest.
2. Good adhesive properties.
3. Good electrical isolation.
4. Mechanical stability.
5. Proper thermal expansion to permit temperature cycling.
6. Chemical stability and inertness.
7. Ease of application.

Several series of epoxies were evaluated early in the program for optical, physical, and chemical properties and the results are given in Table I. The G series was superior to the others tested. The physical, optical, and chemical properties of the G series will now be summarized.

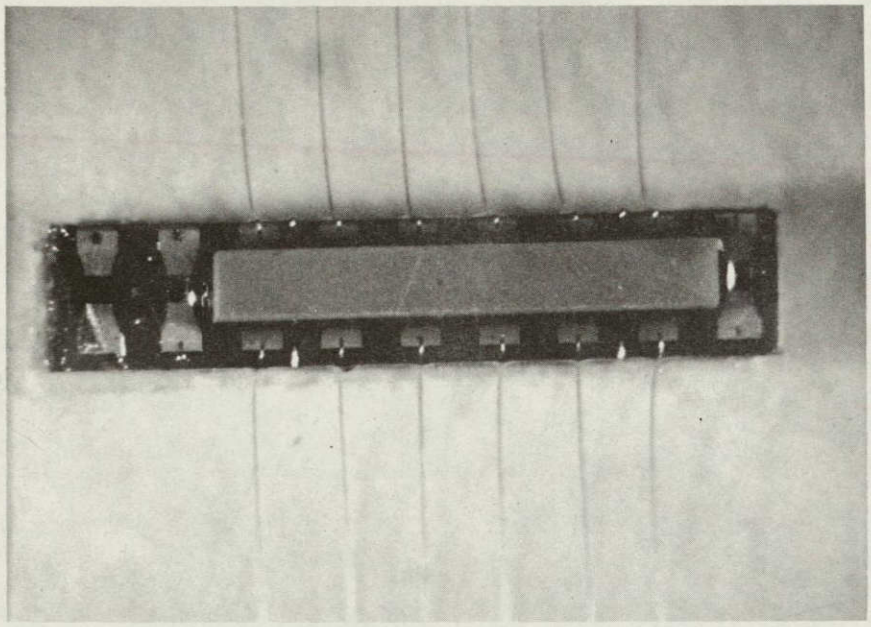

Figure 6 MATERIAL FOR TOP DETECTORS MOUNTED ON FABRICATED BOTTOM DETECTORS

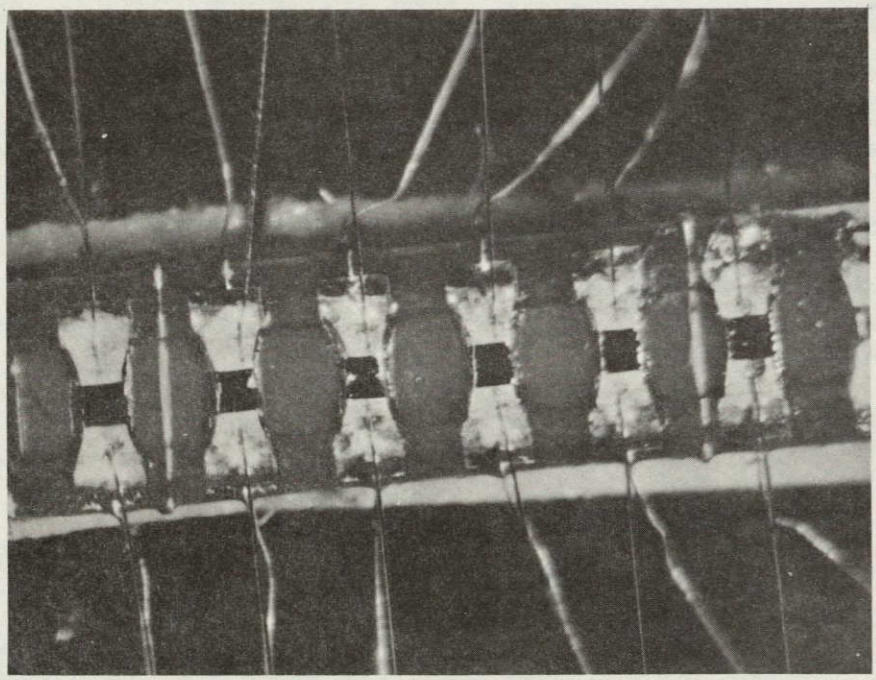

Figure 7 ARRAY OF TWO-COLOR DETECTORS FABRICATED BY ABOVE PROCEDURE

TABLE I

EPOXY CHARACTERISTICS

Honeywell Epoxy	Chemical	Sample Thickness	Transmission Wavelnegth Region (μm)	Transmission Characteristics (%)	Remarks
G	1	light film	see Figure 8		absorption band at 10.9 μm
	2	light film on Irtran II window	see Figure 9		10.9 μm absorption band eliminated. Absorption bands at 9.6 and 12 μm
A	1	1/16" thick sample	2.7 - 3.05 3.7 - 4.15 4.5 - 14.5	≈50 ≈80 None Measurable	Flexible No Adhesion
B	1	1/16" thick sample	2.5 - 14.5	None	Flexible No Adhesion
C	1	5 mil thick sample	2.5 - 2.75 3.8 - 5.6 5.7 - 10 10 - 11.6 12.2 - 14.5	~60 ≈50 None ~7 ≈10	Rigid (Evaluated)
	1	lapped and polished thin film	2.5 - 2.85 2.9 - 3.35 3.7 - 5.6 5.7 - 9.6 10.1 - 11.7 12.4 - 14	≈90 ≈30 ≈60 ≈20 ≈40 ≈35	Dip between 11.8 and 12.3 μm ≈20% transmission
	1	thin film samdwiched between 2 Irtran II windows	2.5 - 7.8 (3.3 - 3.6) 8.0 - 9.5 10.1 - 11.7 12.5 - 14	≈80 - 100 ≈20 ≈50 ≈80 ≈80	Dip between 11.9 and 12.3 μm ~60% transmission
D	1	sandwiched between 2 Irtran II	2.5 - 6 6 - 6.5 7.2 - 8.7 8.7 - 11.1 11.7 - 13.5	~100 100 - 0 ≈0 - 90 ≈80 60 -100	Good resistance to chemicals Epoxy dip at 11.4 - 11.5 Note: IR2 also has broad dip here
E	1	uncured light film	2.5 - 6.4 6.5 - 7.5 8.0 - 9.4 10.0 - 14.0	≈100 ~60 ≈25 ≈70	Dips at 3.4, 5.7, 6.6, 9.6, 10.8 and 11.9 microns Dip at 11.9 microns ≈16% transmission
	2	light film on Irtran II window	2.5 - 4.2 4.5 - 5.5 5.5 - 6.8 7.0 - 8.0 8.0 - 10.0 10.0 - 12.0	≈50 ≈100 ≈60 ≈25 ≈10 ≈70	Dips at 3.5, 5.9, 12.2 (15%)

a) Optical Transmission

The infrared transmission of epoxy G-2 at room temperature for a sample 7.5 μm thick is shown in Figure 8. The epoxy shows a high transmission pass band from approximately 9.8 to 11.8 μm. The same sample was tested for optical transmission at 77 °K and showed no change from that at room temperature. The sample was allowed to age 17 days after cure, and optical transmission properties again were identical at 77 °K as had been previously obtained. Thus the optical transmission characteristics of Epoxy G-2 are very desireable for our purposes in the temperature range of interest.

The optical transmission of Epoxy G-1 was tested on the Beckman IR-7 Spectrometer, and the results are shown in Figure 9. The absorption dip at 10.9 μm makes this chemical form undesirable. However, the epoxy was subsequently modified to eliminate this dip; the result was epoxy G-2.

b) Adhesive Properties

Epoxy G-2 has shown excellent adhesive properties. Scrap detectors were bonded together with G-2 epoxy in a crossed and parallel configuration. The crossed detectors could be separated manually with tweezers only by cracking the detector elements. The parallel detectors could not be separated, attesting to the excellent adhesive strength of the epoxy.

c) Electrical Isolation

The electrical isolation of epoxy G-2 has been found to be good for two-color detectors fabricated in the crossed configuration. Resistance between detectors is greater than 1 megohm as measured with a Wheatstone bridge.

Mechanical Stability and Strength

Epoxy G-2 has also demonstrated excellent properties in this area. Samples 3/8-inch thick cannot be broken manually and exhibit excellent mechanical strength and stability. No cracking has been seen in samples subjected to manual stress.

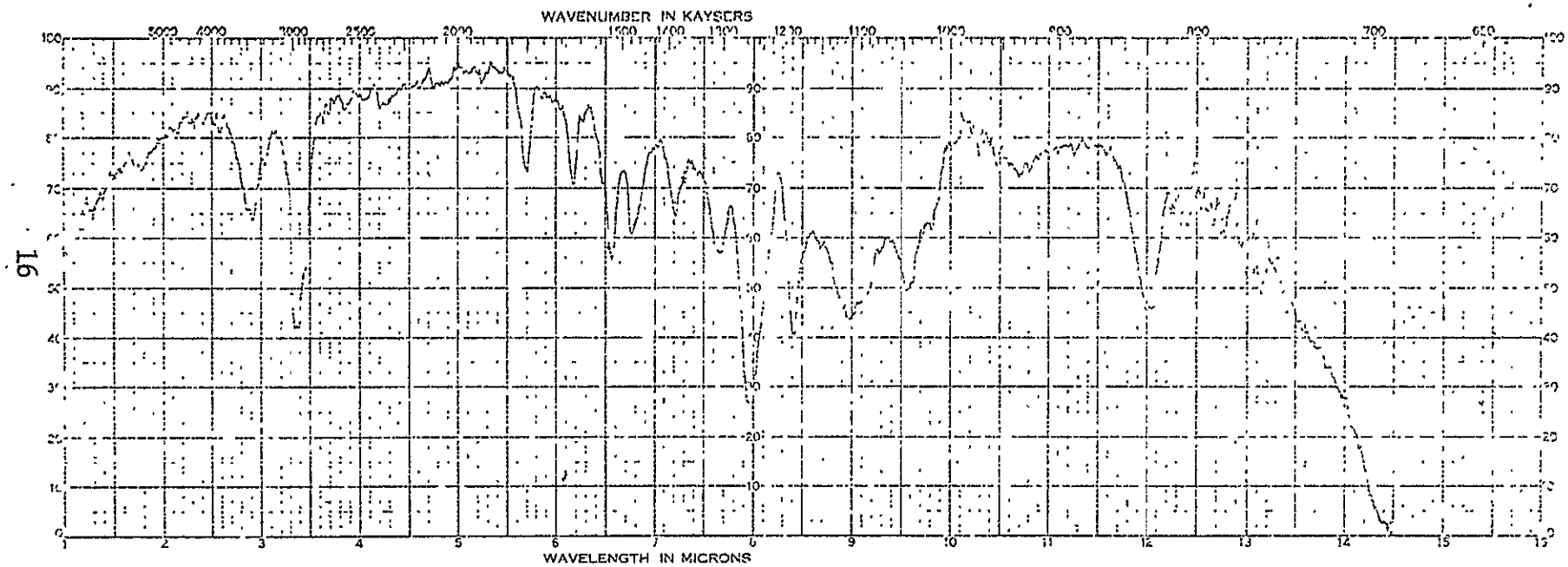

Figure 8 EPOXY G2 (light film) ABSORPTION SPECTRUM

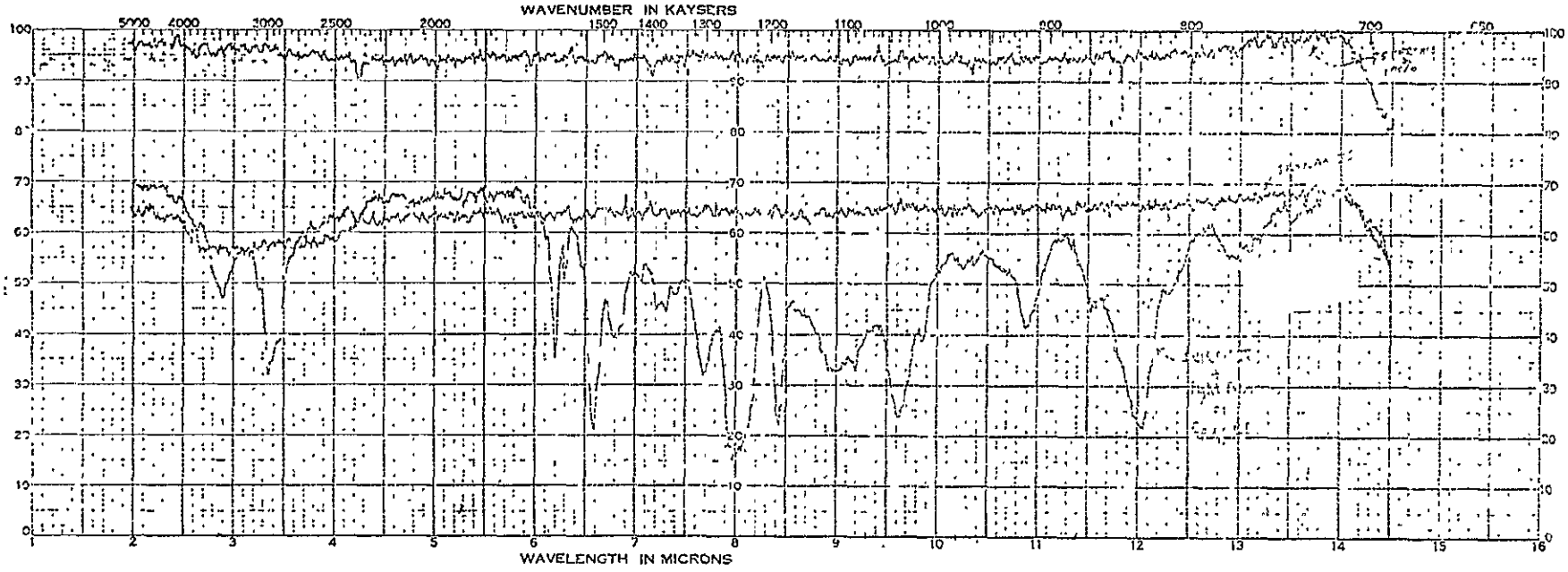

Figure 9. EPOXY at 300 °K

d) Resistance to Temperature Change

Thin layers of epoxy G2 have been tested for resistance to temperature changes. After cure, a thin layer was heated to 65 °C for periods of one day to one week and remained stable and did not become tacky or crack. Thin samples of epoxy G2 on glass slides and two-color detectors fabricated were cycled more than 12 times from room temperature to nitrogen temperatures and the effects on mechanical strength and adhesion noted. The thin samples showed no visible cracking under 40x magnification, and adhesive strength of the two-color detectors remained as previously tested.

Two-color detectors made using the fabrication procedures for the final devices were subjected to 4 °K and 300 °K cycling without cracking or separating.

e) Chemical Resistance Study

Epoxy G-2 has shown chemical stability with time as displayed by the lack of change in the absorption spectra of the newly cured and aged epoxy. The absorption dips identified chemically are invariant with age.

Epoxy G-2 was studied for resistance to chemical solvents used during normal material processing. The basic epoxy resin used was cured with two different curing agents and various percentages of the additive used in epoxy G-2. A filler was also used in G-2 epoxy. All samples were divided into two parts; one was cured at room temperature and the other at elevated temperatures. The cured epoxies were then placed in a typical warm solvent for eight minutes and the percentage increase in weight as well as changes in physical appearance noted. The results of this test are shown in Table II. It can be seen that the additive decreases the ability of the epoxy to resist chemical attack by the warm solvent. The percent weight change increases with increased amount of Additive A. Deterioration of physical appearance (bending and cracking) also increased with increased amounts of Additive A. This additive has been added to Epoxy G specifically to modify the infrared transmission characteristics, i.e., minimize the epoxy dip at 10.9 μm.

Various samples with different amounts of filler were tested for infrared transmission to determine the appropriate tradeoff be-

Table II

CHEMICAL RESISTANCE OF HONEYWELL EPOXY G
(8 minutes in warm solvent)

Honeywell Epoxy G Plus	Curing Conditions	Percent Weight Change	Remarks
Curing Agent A	R.T.	+ 6%	Sweat Spots after cure
	E1	+ 0%	Curled in solvent
Curing Agent A + 5 parts additive A	R.T.	+ 13%	Curled in solvent
	E1	+ 0%	Pock marked surface
Curing Agent B (Epoxy G-1)	R.T.	+ 13%	
	E1	+ 1%	
Curing Agent B + 1 part Additive A	R.T.	+ 8%	Cracked in solvent
	E1	- 4%	
Curing Agent B + 3 parts Additive A	R.T.	+ 15%	
	E1	+ 10%	Bent in solvent
Curing Agent B + 5 parts Additive A (Epoxy G-2)	R.T.	+ 24%	
	E1	+ 22%	Bent in solvent
Curing Agent B + 5 parts Additive A + Filler A	R.T.	+ 5%	Pock marked surface
	E1	+ 7%	from solvent

R.T. = Room temperature
E1 = Elevated temperature

tween infrared transmission and chemical resistance. The results of adding a filler to the Epoxy G-2 are also shown in Table II. Although the epoxy with filler showed more resistance to chemical attack than without filler, the resultant pock marks on the surface made this filler undesireable.

From these facts the percent of additive in epoxy G-2 has been lowered from five parts to three parts resulting in a new epoxy (Honeywell G-3) which so far has shown good resistance to chemical solvents during detector processing and yet maintained the desireable properties of Epoxy G-2 (i.e. good adhesion, ease of application, and high electrical conductance). Two-color detectors, fabricated with a layer of G-3 epoxy (less than 0.0005 inch thick) as the interface epoxy, have shown resistances greater than 9 megohms between top and bottom detectors.

f. Optical Transmission Study

The optical transmission of Epoxy G was studied as a function of various curing times and additives. Very thin (down to 0.001 inch) single film samples were prepared for five different epoxy additive combinations. Each sample was split into two portions, one cured for 6 hours and the other for 30 hours, making a total of 10 samples.

Absorption spectra form 2 through 14.5 μm were run on the Beckman IR 7 spectrophotometer for all ten samples. The transmission at specific wavelengths for each sample was plotted as a function of the sample thickness (measured with a micrometer) for all samples regardless of additives to Epoxy G. One such curve is shown in Figure 10 for 11.3 microns. Figure 10 shows that the main factor in determining the transmission of an epoxy layer is its thickness and that the additives yield only slight variations from the straight line curve. In this manner the epoxy transmission characteristics can be carefully cataloged as a function of layer thickness and wavelength and the absorption coefficient at a specific wavelength calculated. (174 cm^{-1} for the example shown in Figure 10).

g. Ease of Application

Epoxy G-2 is extremely easy to apply and cure, thus making it desireable from a fabrication point of view.

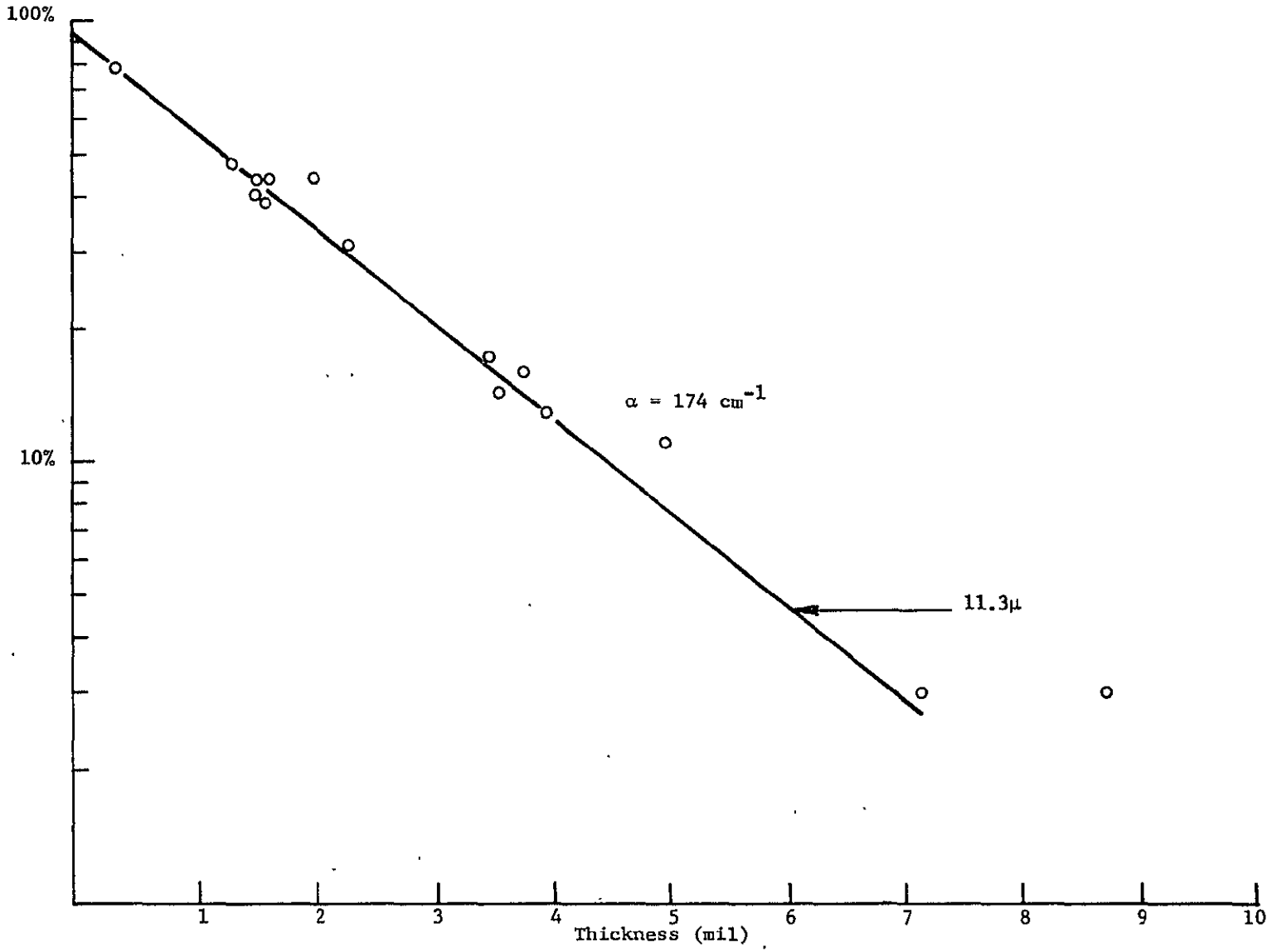

Figure 10 EPOXY TRANSMISSION AT 11.3 MICRONS (SAMPLE IN AIR)

h. Results of the Epoxy Study

From the results of the previous paragraphs, it seems that there is no need for the additive in the epoxy. However, the additive acts as a flexibilizer for the epoxy. Cured epoxy without additive is a means of controlling the thermal expansion properties of the epoxy. The results of the epoxy studies may be summarized as follows:

1. It is the additive in Epoxy G-2 which lowers its chemical resistance.

2. The epoxy thickness is the main factor in determining optimum transmission at and not the additives as previously believed.

3. The main function of the additive is to act as a flexibilizer for the epoxy and thus make it capable of withstanding nitrogen temperatures.

2.1.4 Direct Coating of Optical Filters on Detector Surfaces

Four detectors were sent to OCLI in an attempt to directly coat optical filters on detector surfaces. These detectors have been evaluated and the effects of the blackbody D* are listed in Table III. Only one detector C6) appears to have survived the coating process. Two other detectors exhibited a marked degradation in D* performance. A fourth element was returned from OCLI with a severed contact area and a missing lead and thus could not be evaluated. Element C6 was tested for spectral response and the resulting curve is shown in Figure 11. The detector with the coated filter exhibits a cut-on at 10 μm and optical leaks of more than 20% at wavelengths less than 8 μm. The other two detectors could not be tested for spectral response due to their D*, and attempts to find a strong signal in the 8-14 μm bandpass filter on the detector surface was not successful. However, the fact that one detector survived the process suggests possible success in future efforts where appropriate modifications have been made.

This approach was not be pursued further during the present program; however, later this concept should be investigated because its feasibility was successfully demonstrated in at least one detector.

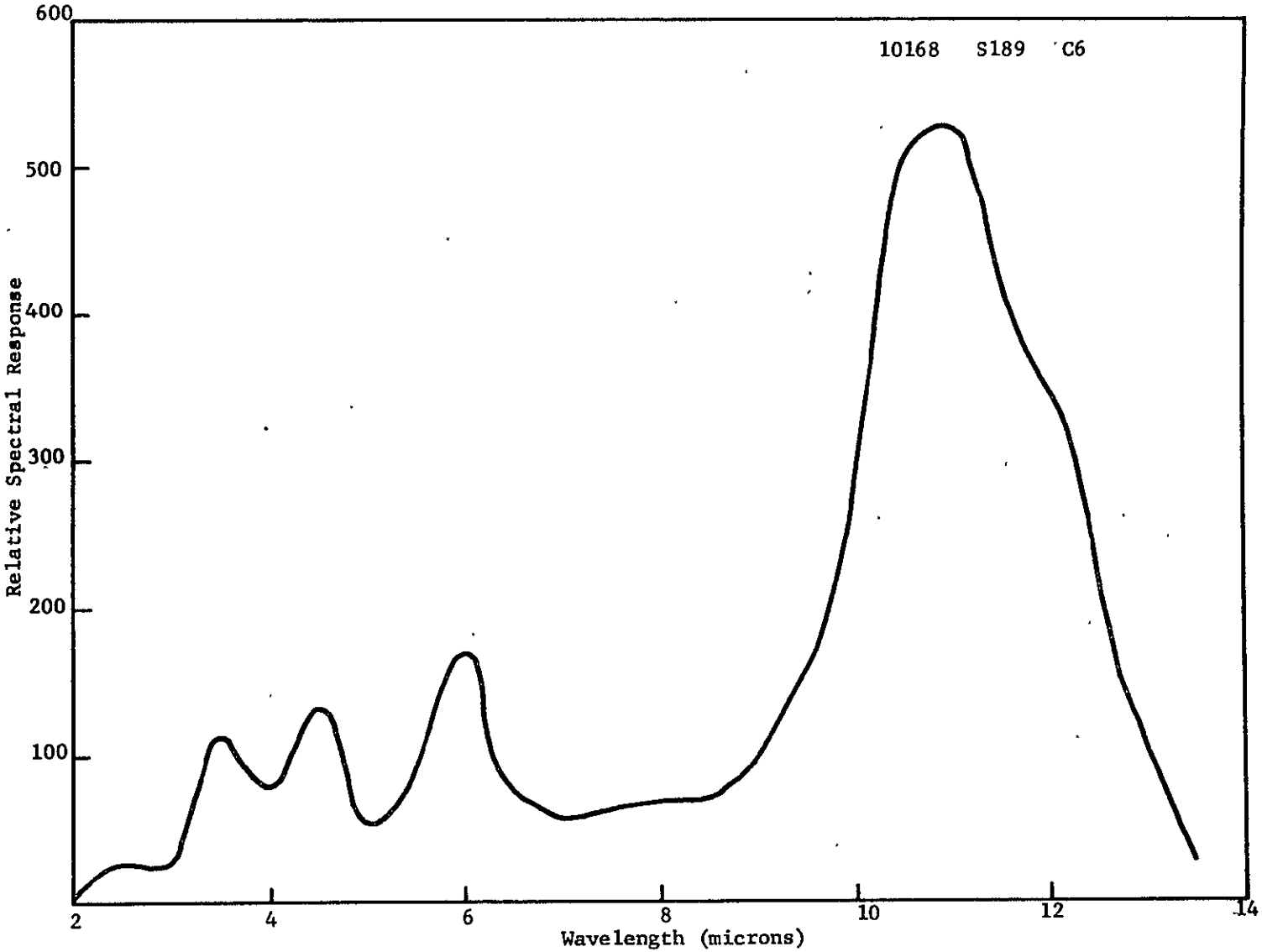

Figure 11 AFTER OCLI COATING

Table III

	D^*_{bb} (500,1000,1) before coating	D^*_{bb} (500,1000,1) after coating
C6	1.6×10^9	1.5×10^9
D5	2.7×10^9	5.5×10^8
D6	5.1×10^9	2.7×10^8

2.2 Two-Color Detector Performance

2.2.1 Introduction

Two-color (Hg,Cd)Te photoconductors can provide high spectral detectivities in both channels. Of course, the top element experiences neither enhancement or degradation of detectivity in this configuration. For the bottom element the situation is more complex; enhanced spectral detectivities occur with high performance material and degradation of the spectral detectivity results from low performance material. The responsivity is always degraded when the detector is made into the bottom element of a two-color detector due to absorption and reflection losses. However, the noise may be reduced also because the top detector acts as a cooled cut-on filter. If the detector is fully BLIP, then the specific detectivity can be enhanced. This effort is demonstrated by the data in Figure 12 which shows the spectral detectivity of a detector as a single element and as the bottom element of a two-color detector. The peak spectral detectivity is greater for the detector as the bottom element of the two-color than as a single element.

2.2.2 Two-Color Detector Uniformity

(Hg,Cd)Te material is characterized by excellent uniformity. The fabrication procedure described in Section 2.1 showed the preselection process for top element detector material and the selection method for bottom detector elements. Data for a plank cut from the ingot grown for this program is shown in Figure 13. Four rows from this plank were evaluated and sections in each row were suitable for the fabrication of top elements for the present

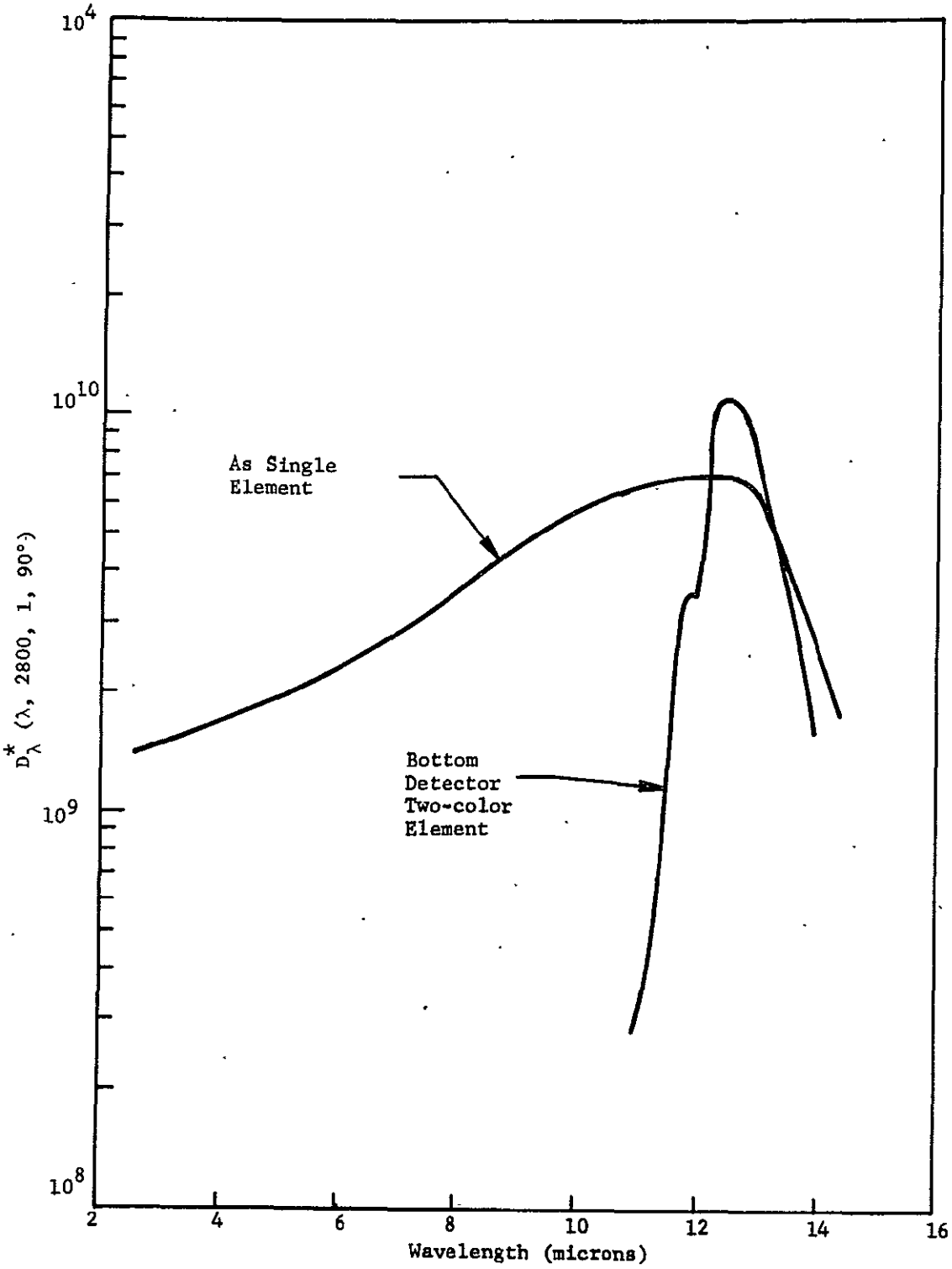

Figure 12 DETECTIVITY VS WAVELENGTH FOR BOTTOM DETECTOR

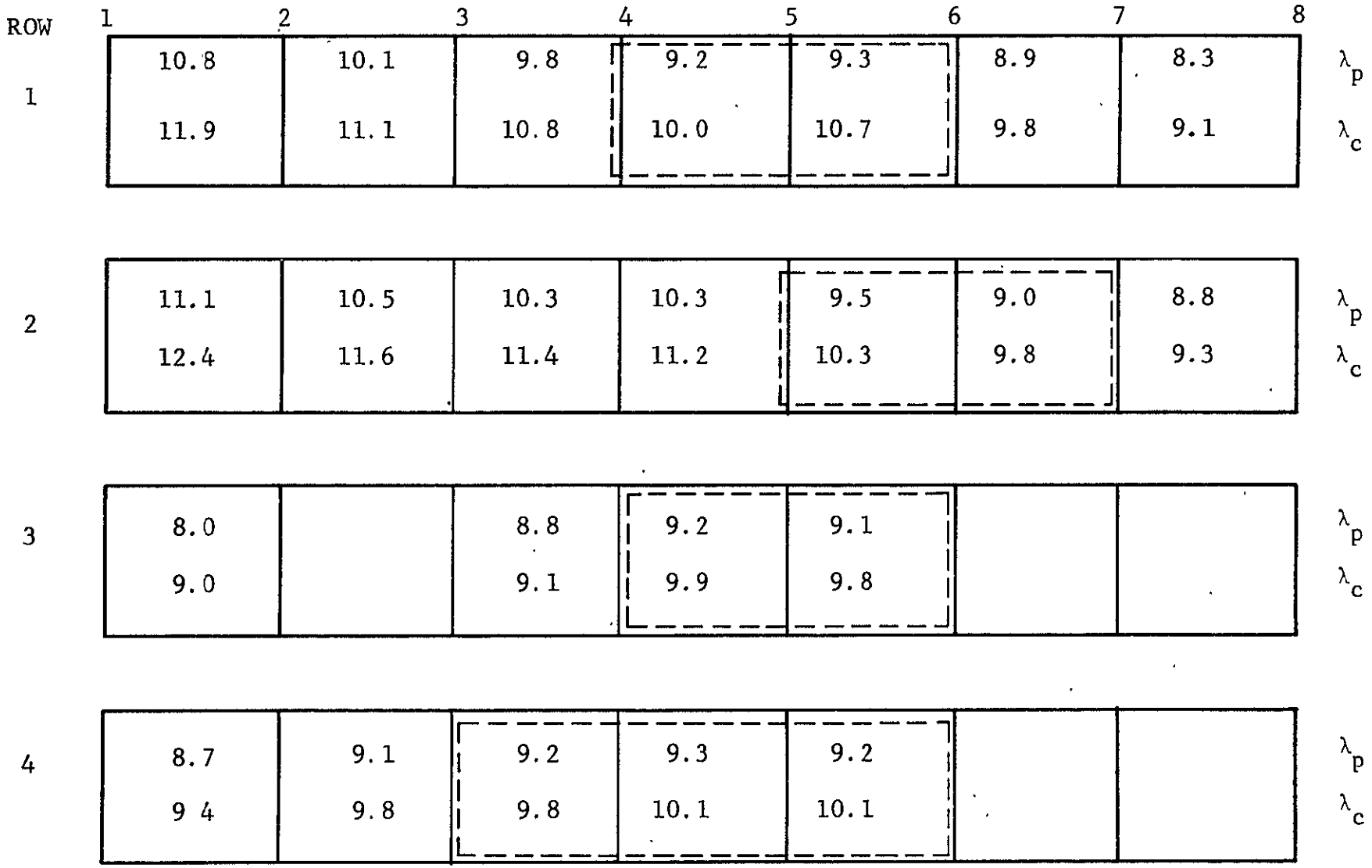

Figure 13 SPECTRAL RESPONSE DATA FOR TWO ROWS OF DETECTORS TO BE USED FOR THE BOTTOM ELEMENTS OF TWO-COLOR DETECTORS

program. Each section would provide a many-element array as discussed in Section 2.1. Good uniformity for bottom elements is shown by the spectral data in Figure 14. This demonstrates that (Hg,Cd)Te material possesses the uniformity required to produce two-color detectors with good uniformity in high yield for small cutoff wavelength tolerances. Good uniformity for bottom elements is demonstrated by the spectral data in Figure 14 for an array of bottom element detectors.

2.2.3 Two-Color Detector Array Performance

Performance data for a six-element array fabricated from Row 1, Slab 145 on top of Slab 182, Row B is given in Table IV. A typical spectral response is shown in Figure 15 for element No. 10. The active area of the elements was 0.010 inch by 0.010 inch. Detector No. 10 top had a D^*_λ (λp, 10 kHz, 1) of 1.19×10^{10} cm $Hz^{1/2}$/Watt and a cutoff wavelength at 8.9 μm. The bottom element had a D^*_λ (λp, 10 kHz, 1) of 7.7×10^9 cm $Hz^{1/2}$/Watt^{-1} with a cutoff wavelength of 11.2 μm. The short wavelength edge of the optical bandpass of the bottom detector was 9.9 μm.

The electrical isolation between top and bottom detectors was determined from the electrical resistance which was greater than 9 megohms.

2.2.4 Performance of Top and Bottom Detectors as Single Elements

Detectors were fabricated from Row B of Slab 182 for use as bottom elements. The single element showed good D^*_{bb} values. The values are tabulated in Table V along with values of peak wavelength, cutoff wavelength, and detector resistance.

The results for seven other detectors from the same row are tabulated in Table VI. In addition to the data given for the above detectors, the values for the responsive time constant τ_R and for the 1/f knee frequency K 1/f are given; that is, the frequency at which the extrapolated generation-recombination noise occurs. These seven detectors have been fabricated into an array of two-color detectors.

Material suitable for fabrication of the top detectors was evaluated for cutoff wavelength using the spectral response as described in Section 2.3. The peak wavelength and cutoff wavelengths are shown in Figure 16. Piece 1 was used to fabricate the two-color detectors described in the previous section. Piece 2 was used for fabrication of the second two-color array. Two

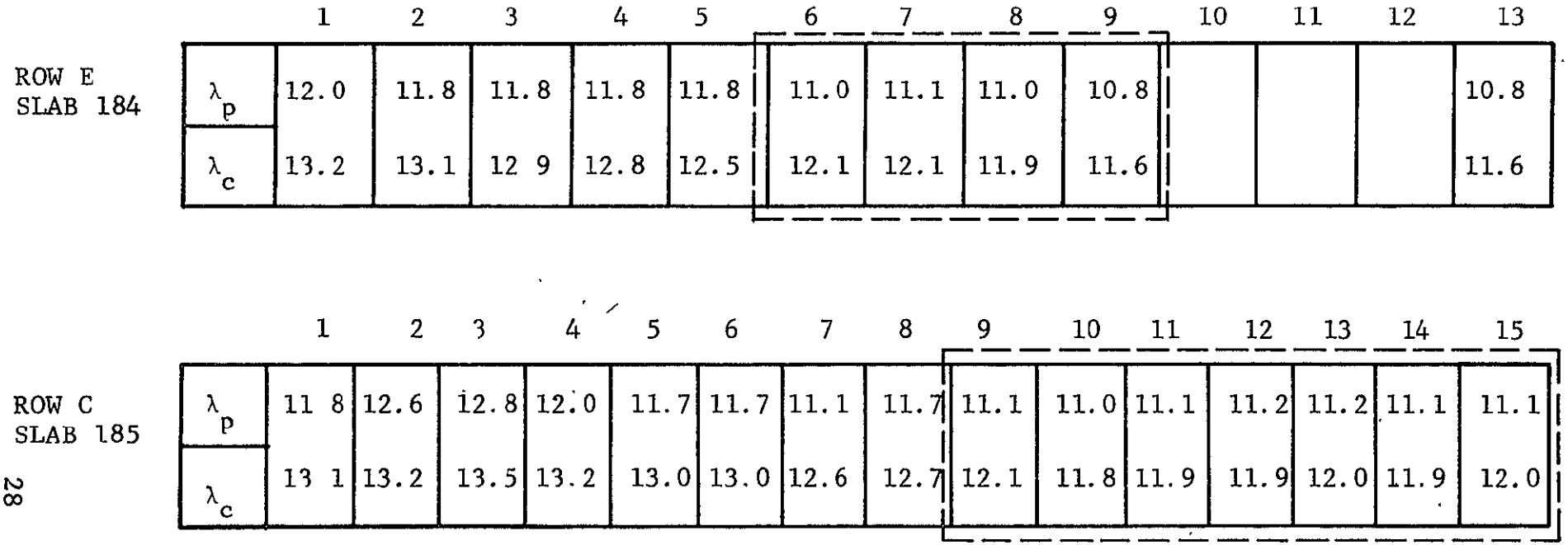

Figure 14 SPECTRAL DATA FROM FOUR ROWS OF PLANK 4 - TOP ELEMENTS

Table IV

PERFORMANCE DATA OF TWO-COLOR ARRAY -
SLAB 145, PIECE 1, SLAB 182, ROW B

Two-color array data (78°K) FOV = 100 °

	Top Detector					Bottom Detector					
Element	λp	λ_{co} microns	D^*_λ ($\times 10^9$)	τ_d	τ ns	λ_p microns	λ_{co}	$\Delta\lambda$	D^*_λ ($\times 10^9$)	τ_d	τ ns
9	8.3	8.7	7.0	577		10.2	10.9	1.1	8.1	730	-
10	8.1	8.9	11.9	565	535	10.3	11.2	1.3	7.7	110	178
11	8.5	9.1	1.3	2500	-	10.1	10.8	1.0	5.5	765	-
12	8.3	9.1	6.0	755	-	10.2	11.0	1.3	4.6	485	-
13	8.9	9.4	4.1	560	-	10.2	10.9	1.2	7.5	235	-
14	8.9	9.4	4.7	700	-	10.3	10.9	1.0	5.5	580	-

(a) does not include leak correction factor

Table V

PERFORMANCE OF ROW B DETECTORS
TESTED AS SINGLE ELEMENTS PRIOR
TO ADDITION OF TOP ELEMENT

Element	$D^*_{bb} \times 10^9$ (cmHz$^{1/2}$/watt)	λ_p (microns)	λ_{co} (microns)	r_d (ohms)
9	6.3	10.3	10.9	520
10	5.67	10.2	11.3	75
11	7.0	10.3	11.0	565
12	8.15	10.7	11.1	325
13	7.32	10.3	11.4	225
14	6.95	10.3	11.0	680

Table VI

PERFORMANCE OF
ADDITIONAL ROW B. DETECTORS

Element	K1/f	$D^*_{bb} \times 10^9$ (cmHz$^{1/2}$/watt)	λ_p microns	λ_{co} microns	r_d ohms	τ_R nanoseconds
1	4	6.32	10.8	12.1	540	158
2	9	6.3	11.0	12.3	170	105
3	6	6.5	10.5	12.1	130	132
4	2.7	5.45	11.0	12.0	240	145
5	6.5	6.16	11.0	11.9	165	122
6	5	5.05	11.0	12.2	80	122
7	6	6.25	10.5	11.2	240	198

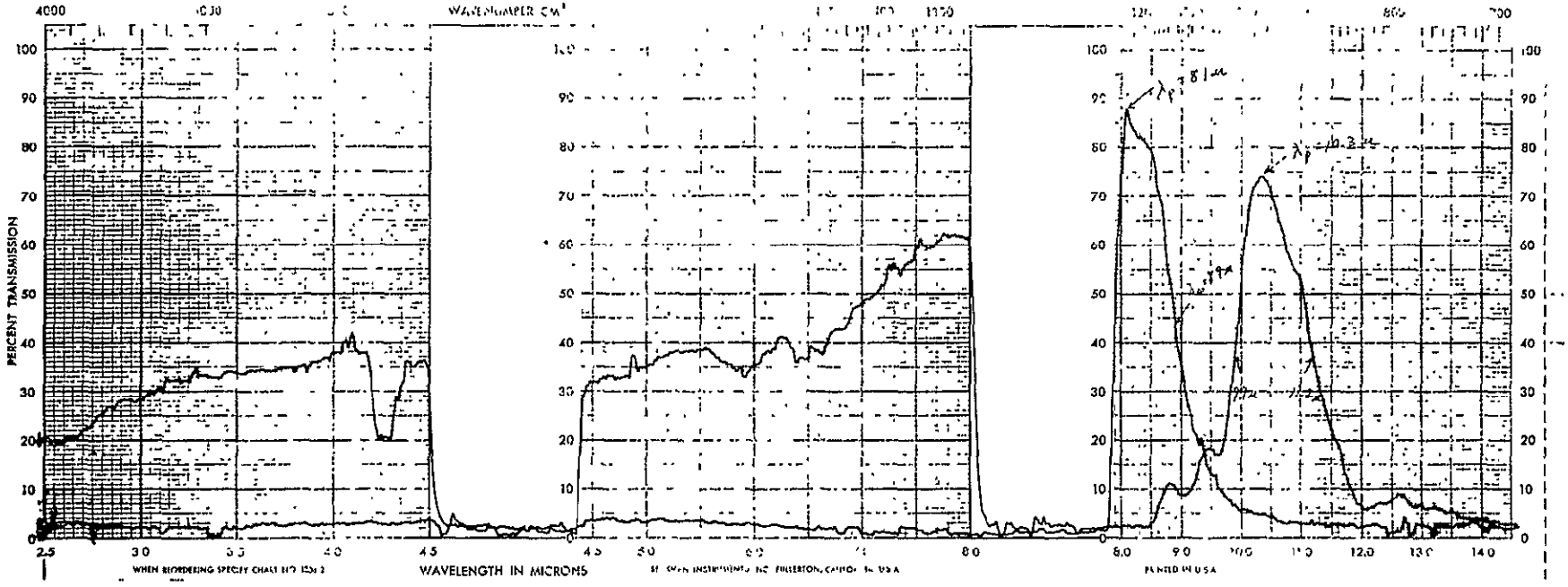

Figure 15 SPECTRAL RESPONSE OF TWO-COLOR DETECTOR NO. 10

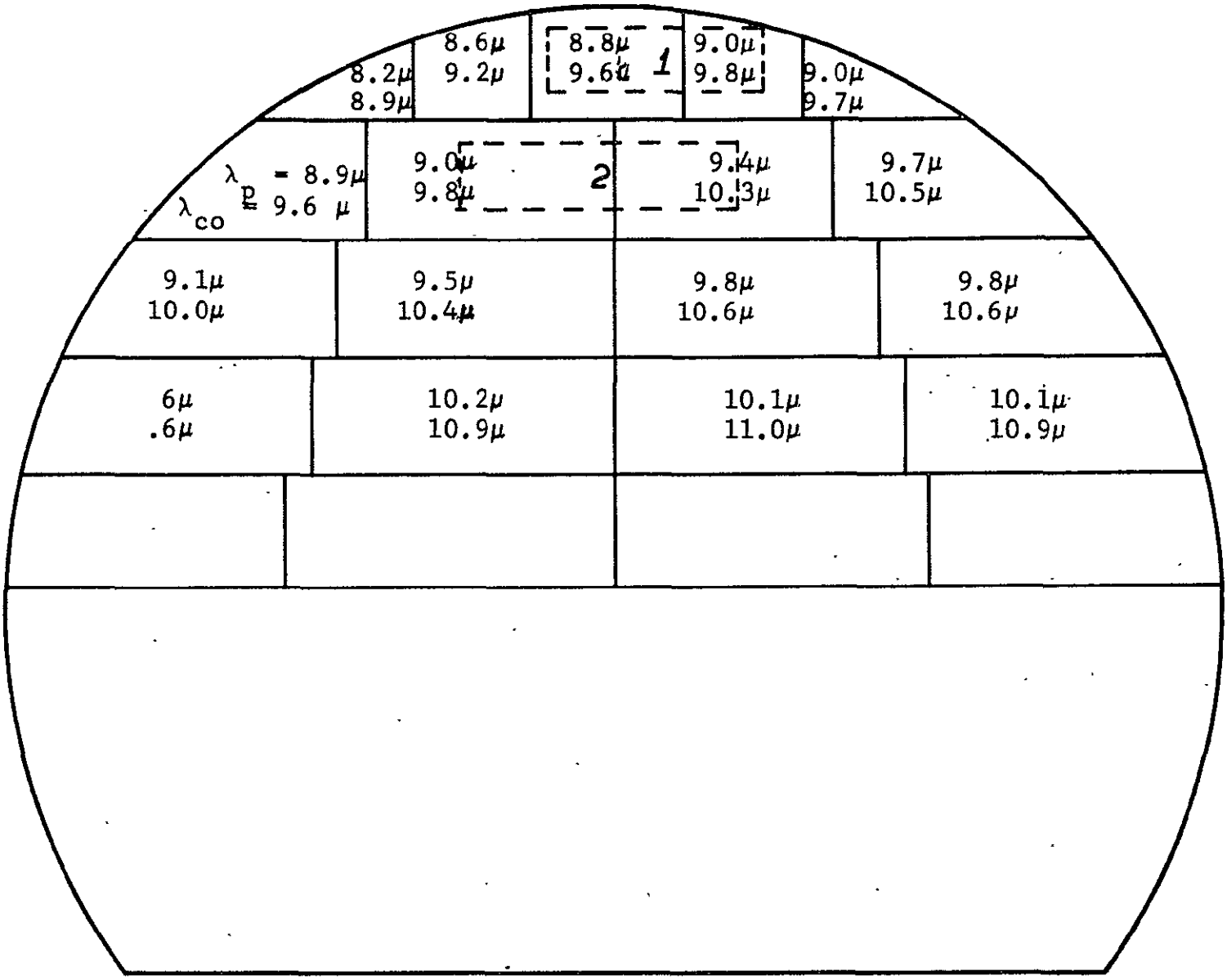

Figure 16. SPECTRAL RESPONSE OF SLAB 145 TO DETERMINE REGIONS OF PROPER WAVELENGTH FOR TOP DETECTORS

elements from this array were delivered to NASA/GSFC as delivery items for the contract; the performance data are given in Section 3.

2.2.5 Two-Color Detector Performance at Elevated Temperatures

Detectivity, spectral response, device resistance, and noise spectra measurements were taken at five temperatures from 82 °K to 120 °K for one two-color detector of the array fabricated. The results of these measurements are listed in Table VII. The top detector exhibited a peak detectivity of 1.94×10^{10} cm $Hz^{1/2}$/Watt at 90 °K for a field-of-view of 60 degrees at 10 kHz while the peak specific detectivity for the bottom detector is 5.9×10^{9} cm$Hz^{1/2}$/Watt at 82 °K under the same test conditions. Detectivity as a function of temperature is plotted in Figure 17 and the shape elements studied during the 12 μm 120 °K and 105 °K, 15 μm program sponsored by NASA/Goddard (Contracts NAS 5-11554 and NAS 5-21068). At 95 °K through 120 °K the specific detectivities measured at 10 kHz exceed the design goal of the two-color program. However, the cutoff wavelength of the top detector is 0.6 μm shorter than the design goal, while that of the bottom is 0.7 μm shorter, although the bandwidth of 0.8 μm is within the design goal of 1.2 μm. While it can be seen from Table VII that the cutoff wavelength of the top detector decreases as expected with increasing temperature, the peak wavelength of the bottom element is less sensitive to temperature change. This is due to the epoxy designed for the interface layer. The epoxy absorption band 9.6 μm defines the cut-on of the bottom detector as more than or equal to 9.9 μm so that the two-color detector exhibits the desired ozone rejection.

2.2.6 Noise Spectra of Two-Color Detectors at Elevated Temperatures

Noise spectra were taken for the top and bottom detectors at each of the five temperatures from 82 °K to 120 °K, and the results for the bottom detector at 80 °K and 120 °K are shown in Figure 18 a-e for detector 10b. The lifetime τ_{pc} is plotted as a function temperature in Figure 19 for the bottom detector. This curve is consistent with previous studies for NASA/Goddard which showed a peak lifetime at approximately 100 °K, Shockley-Read dominated recombination at lower temperatures, and Auger recombination at temperatures greater than the peak.

Table VII

TWO-COLOR DETECTOR PERFORMANCE OUTPUT AT ELEVATED TEMPERATURE

Variable Temp. Data (No. 10) FOV = 60°

	Top Detector							Bottom Detector					
Temp. (°K)	λp	λ_{co} microns	$D_{\lambda}{}^{9}$ (x 10^9)	r_d	τ_r	k_f (kHz)	λp (microns)	λ_{co}	$\Delta\lambda$ (microns)	$D_{\lambda}{}^{9}$ (x 10^9)	r_d	τ	k_f
82°K	8.3	8.9	16.9	650	535	13	10.3	11.2	1.4	5.9	100	178	8
90°K	8.3	8.8	19.4	560	400	20	10.2	10.7	1.0	5.1	90	200	13
95°K	8.2	8.7	18.3	535	400	30	10.1	10.6	.8	4.3	82	230	2.5
105°K	8.0	8.6	12.7	395	590	20	10.1	10.6	.8	3.5	70	265	8
120°K	7.7	8.4	8.3	235	750	10	10.1	10.5	.8	2.7	49	245	10

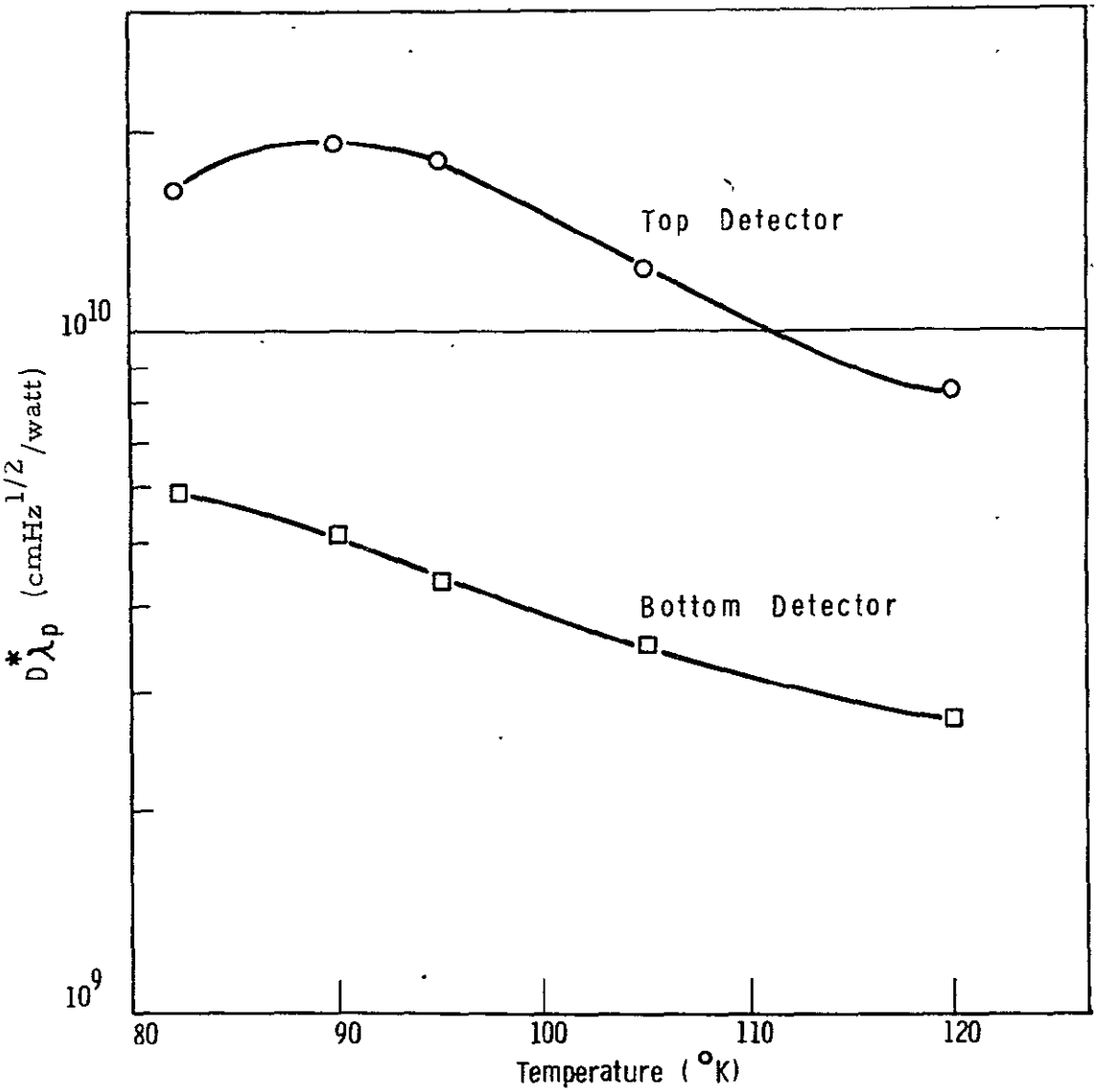

Figure 17 PEAK DETECTIVITY VS TEMPERATURE FOR A TWO-COLOR ELEMENT

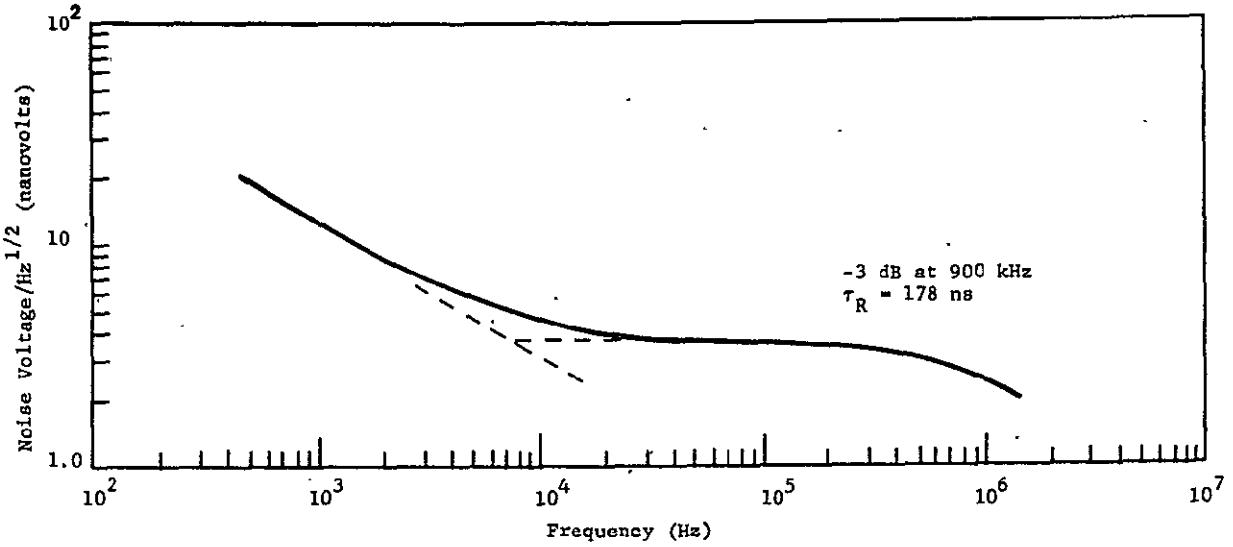

Figure 18a NOISE VOLTAGE VS FREQUENCY FOR 10B AT 81°K

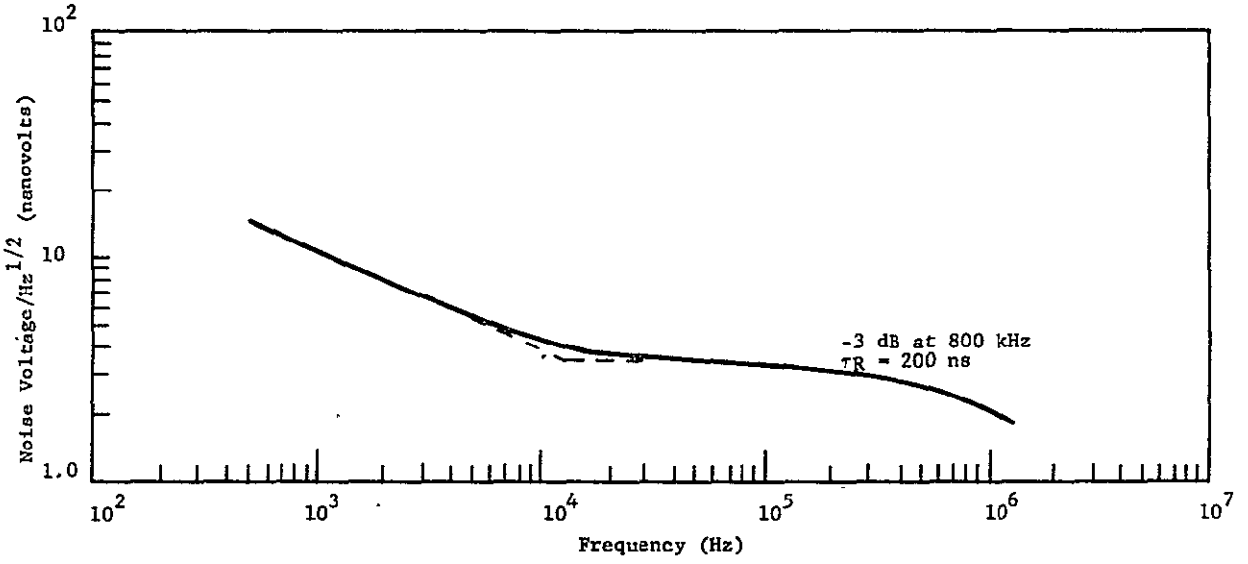

Figure 18b NOISE VOLTAGE VS FREQUENCY FOR 10B AT 90°K

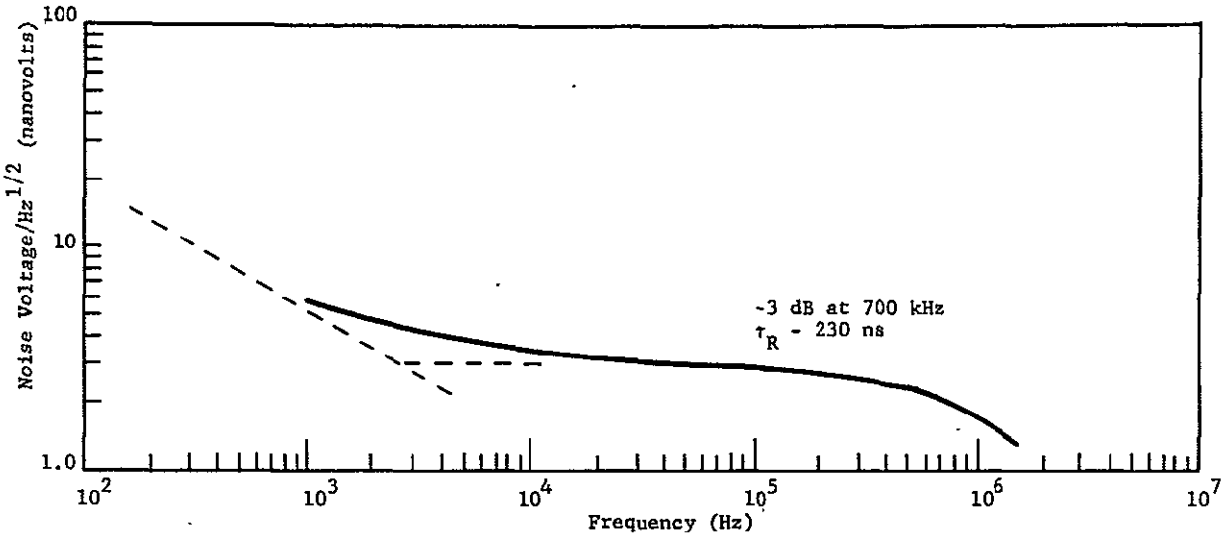

Figure 18c NOISE VOLTAGE VS FREQUENCY FOR DETECTOR 10B AT 95°K

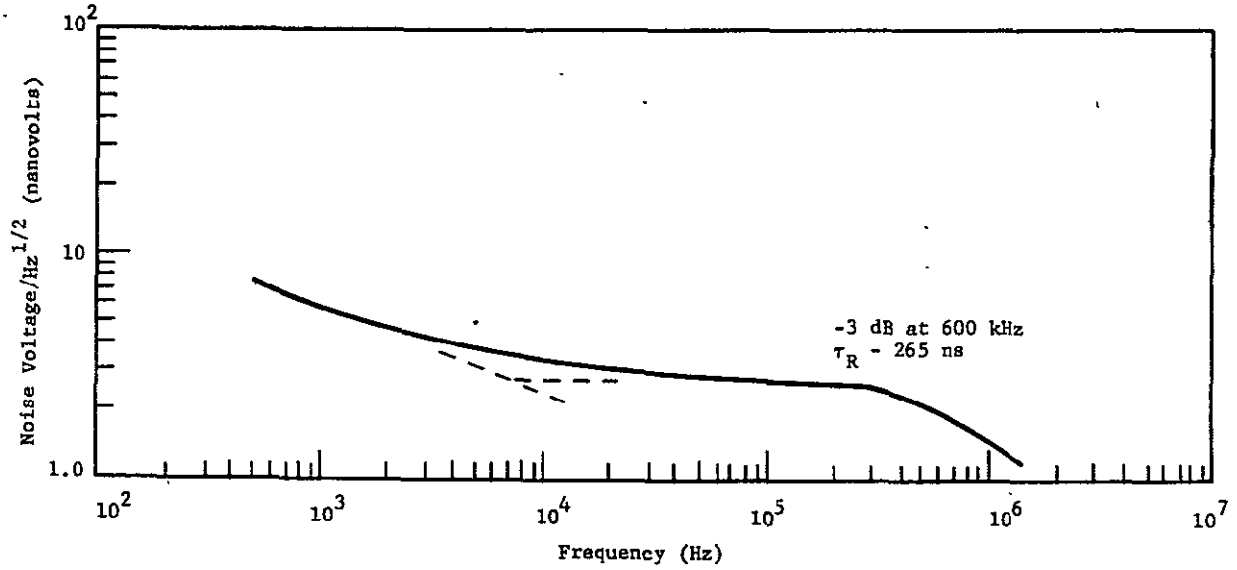

Figure 18d NOISE VOLTAGE VS FREQUENCY FOR DETECTOR 10B AT 105°K

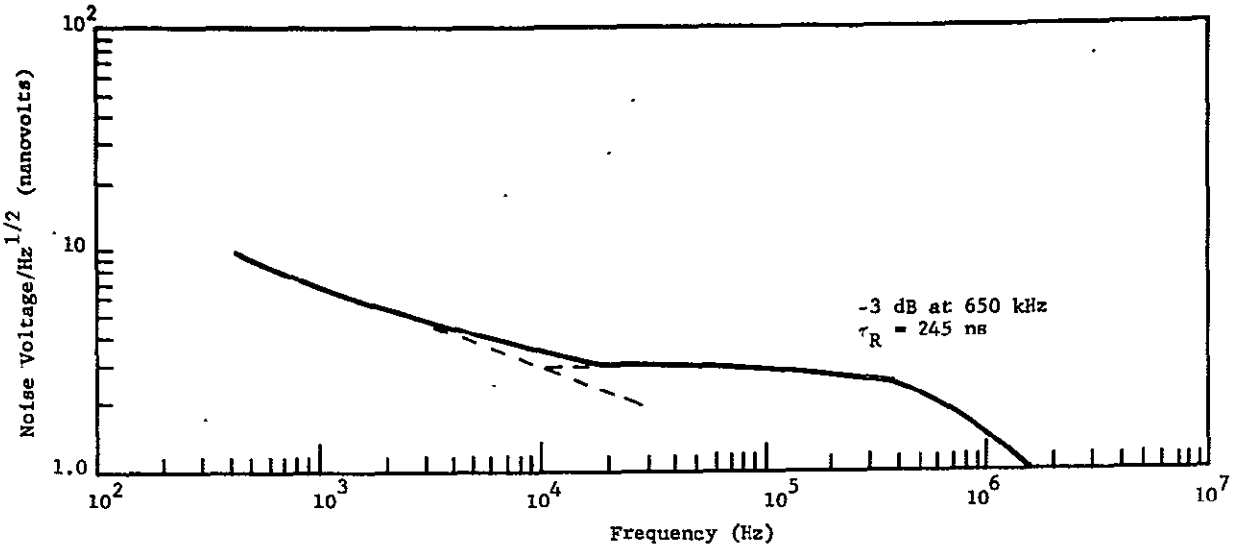

Figure 18e NOISE VOLTAGE VS FREQUENCY FOR DETECTOR 10B AT 120 °K

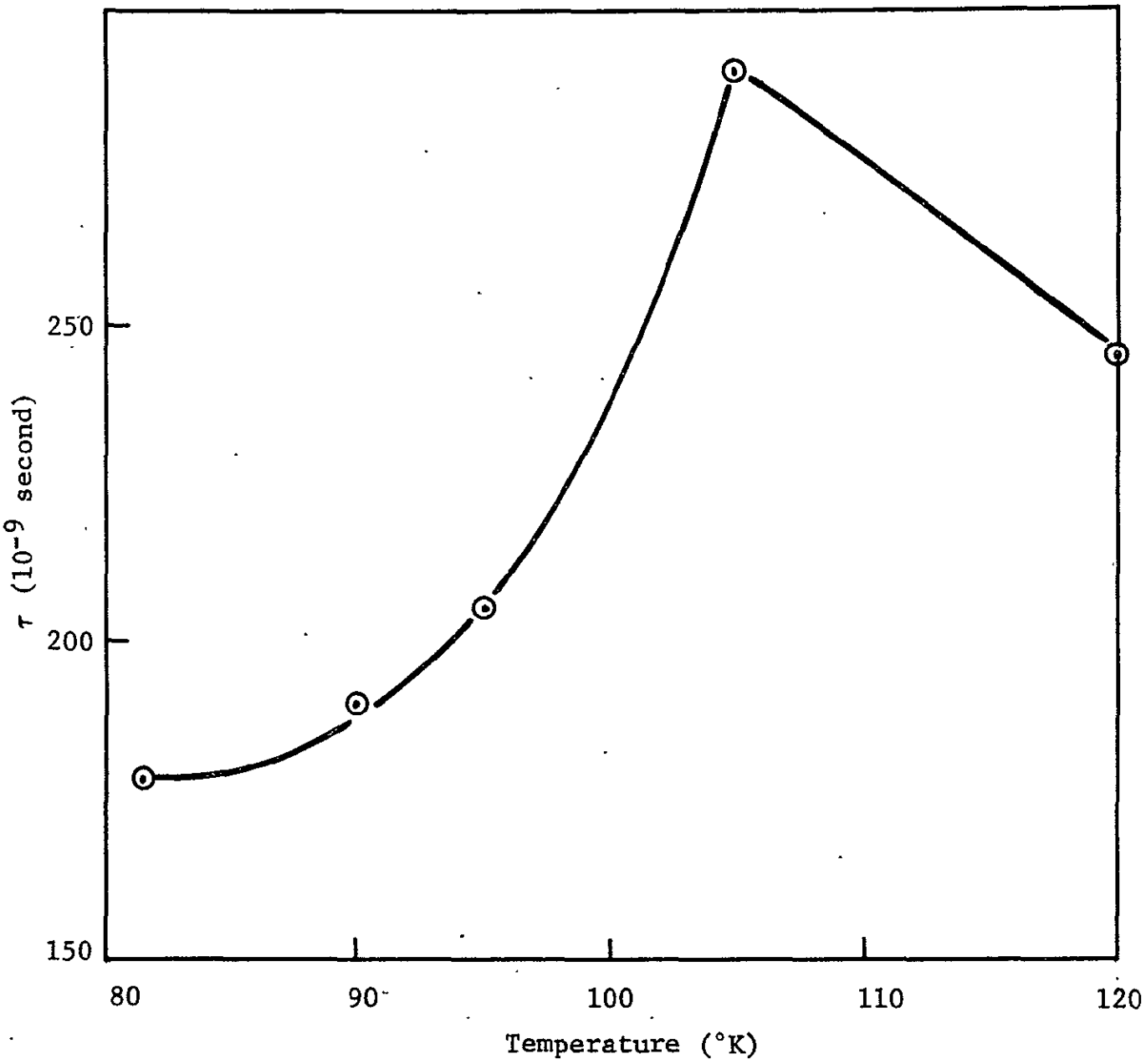

Figure 19 LIFETIME VS TEMPERATURE FOR DETECTOR 10B

The 1/f knee, where the 1/f noise and the g-r noise intersect is in the 3-10 kHz for the bottom detector. The 1/f noise was not measured before being made into a two-color detector, so from this detector it is not possible to determine whether the 1/f noise increased. However, the value of the 1/f knee suggests that the excess noise did not increase since 3-10 kHz is a typical value for K 1/f in single-element detectors. A detailed discussion of 1/f noise is given in Section 2.2.7.

2.2.7 1/f Noise in (Hg,Cd)Te Detectors

The (Hg,Cd)Te photoconductors exhibit a classic noise spectrum as shown in Figure 20 where the low frequency performance is limited by the 1/f noise voltage. Previous work performed at the Honeywell Radiation Center (summarized in the report of Contract NAS 1-8996) has established the relationship between 1/f noise and the sample resistivity.

Low frequency noise may be defined either in terms of the 1/f knee frequency or following: Kruse et al the 1/f noise constant C_1. Then:

$$V_{1/f}^2 = \frac{K_{1/f} V_{gr}^2 \Delta f}{f^\beta} = \frac{C_1 I^2 R^2}{\ell A} \cdot \frac{\Delta f}{f^\beta}$$

where

$K_{1/f}$ = 1/f knee frequency (measured)

C_1 = a factor dependent upon material but independent of dimensions; ℓ the detector length and A the cross-sectional area

V^2_{gpr} = generation-recombination noise voltage

I = the bias burrent

R = the sample resistance

Δf = the electrical bandwidth

β = the exponent of the frequency dependence which is approximately 1

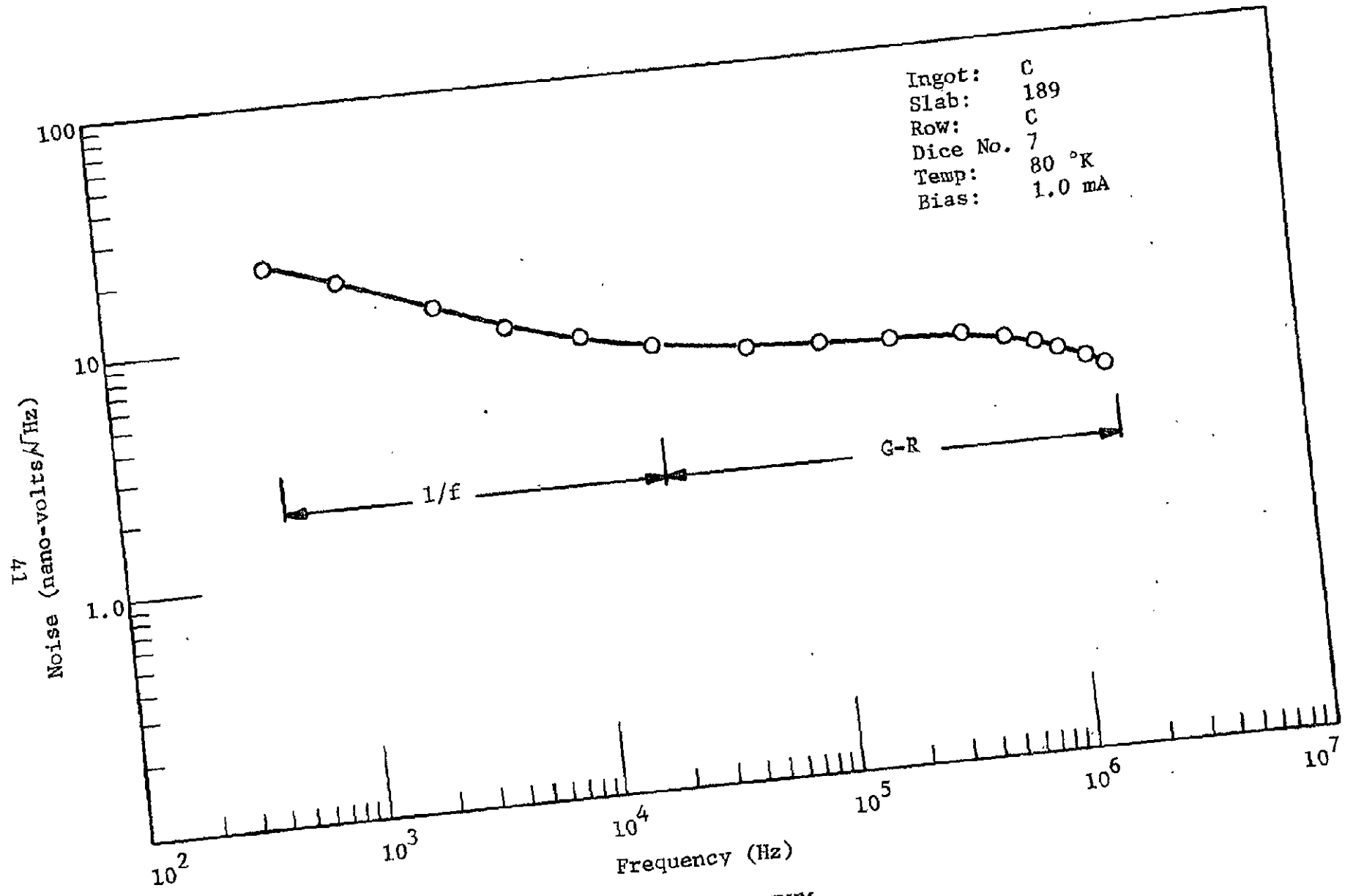

Figure 20 NOISE SPECTRUM

The 1/f noise voltage can be expressed in terms of the element resistivity ρ:

$$V_{1/f}^2 = \frac{C_1 \rho^2 I^2 \ell}{f A^3} \Delta f$$

so that,

$$C_1 = \frac{V_{1/f}^2 f A^3}{\rho^2 I^2 \ell \Delta f} = K_{1/f} \ell A \frac{V_{gr}^2}{I^2 R^2}$$

Experimentally, two cases for the dependence of C_1 on ρ have been found. When $\rho \leq 0.4$ ohm cm, the dependence is approximately

$$C_1 \sim \rho^{+5/2}$$

whereas in higher resistivity, material C_1 seems to be invariant with ρ. Thus, low resistivity material gives lower 1/f noise. This is shown in Figure 21 which includes data from other programs.

We have calculated C_1 and ρ for detector No. 10 top and No. 10 bottom. The values are for No. 10 top: $\rho = 0.5$ and $C_1 = 2.5 \times 10^{-17}$; for No. 10 bottom $\rho = 3.5$ and $C_1 = 5.8 \times 10^{17}$. These data points are shown in Figure 21 for No. 10 bottom and No. 10 top. The data is consistent with previous data.

Low resistivity material is generally associated with classical n-type material, whereas higher resistivity is generally associated with either compensated material or p-type material with an n-type skin. This may explain some anomalous behavior and also low detectivities.

The situation has been clarified recently by W. Scott and R. Hager (J. Appl. Phys. 42 804, 1971) who made a detailed study of the Hall coefficient and resistivity in (Hg,Cd)Te as a function of temperature. Three types of (Hg,Cd)Te were characterized: (1) classical n-type material, and (2 and 3) anomalous material, which was shown by Scott and Hager to be due to p-type material with n-type skin. The Hall coefficient and resistivity as a function of temperature for the three types of material are shown in Figures 22 and 23.

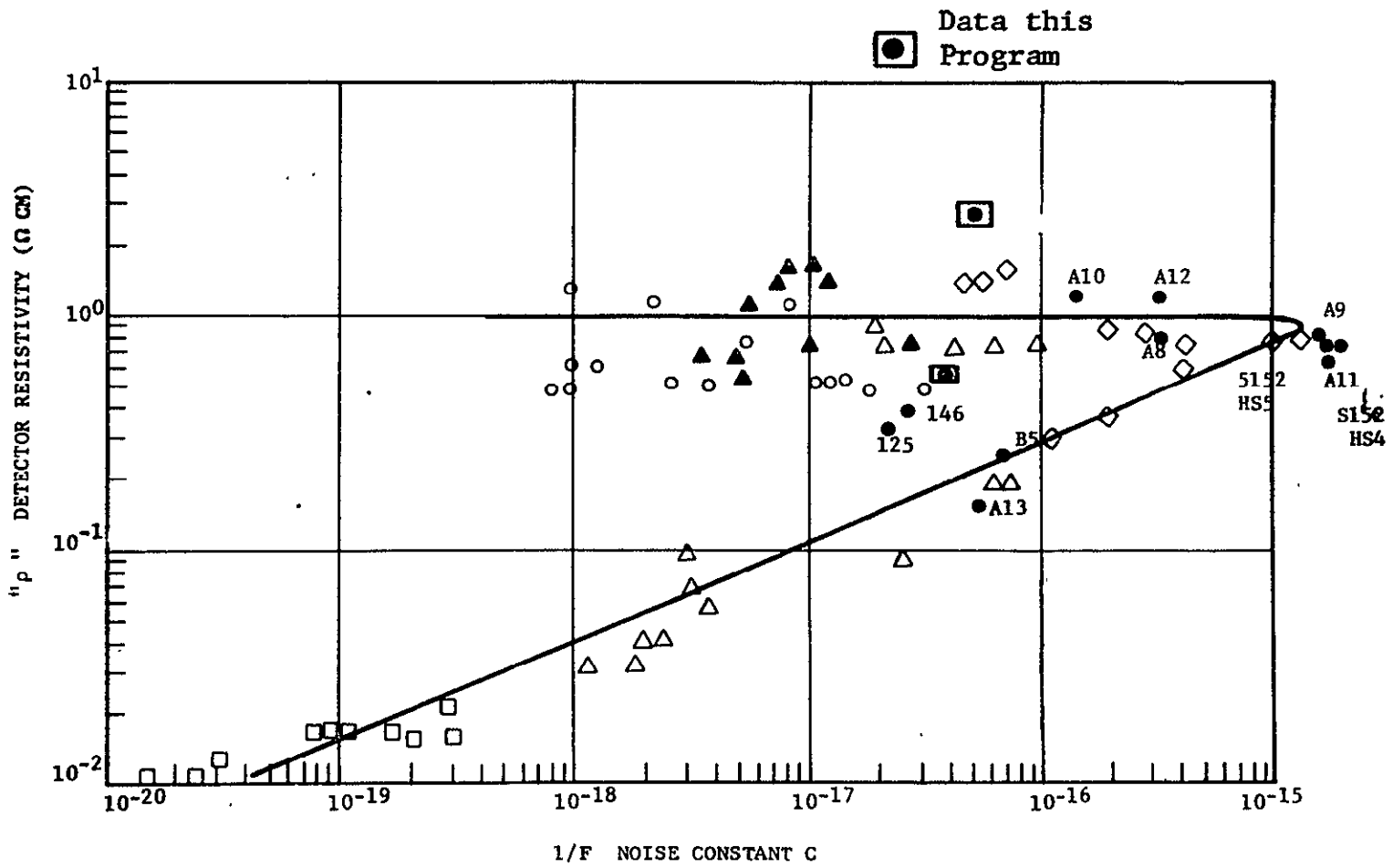

Figure 21 ρ VERSUS 1/f CONSTANT "C"

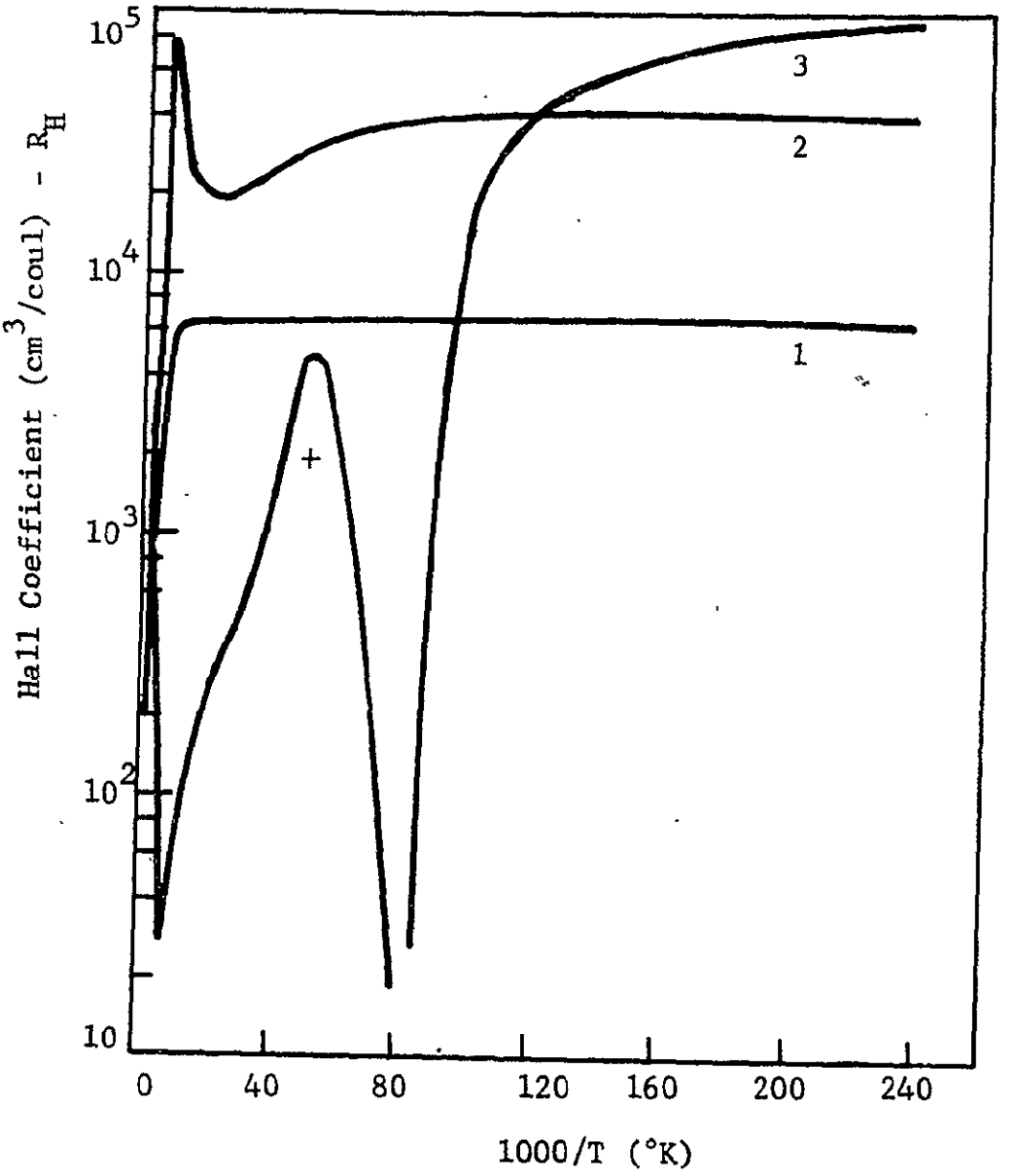

Figure 22 ANOMALOUS BEHAVIOR OF R_H AS FUNCTIONS OF TEMPERATURE

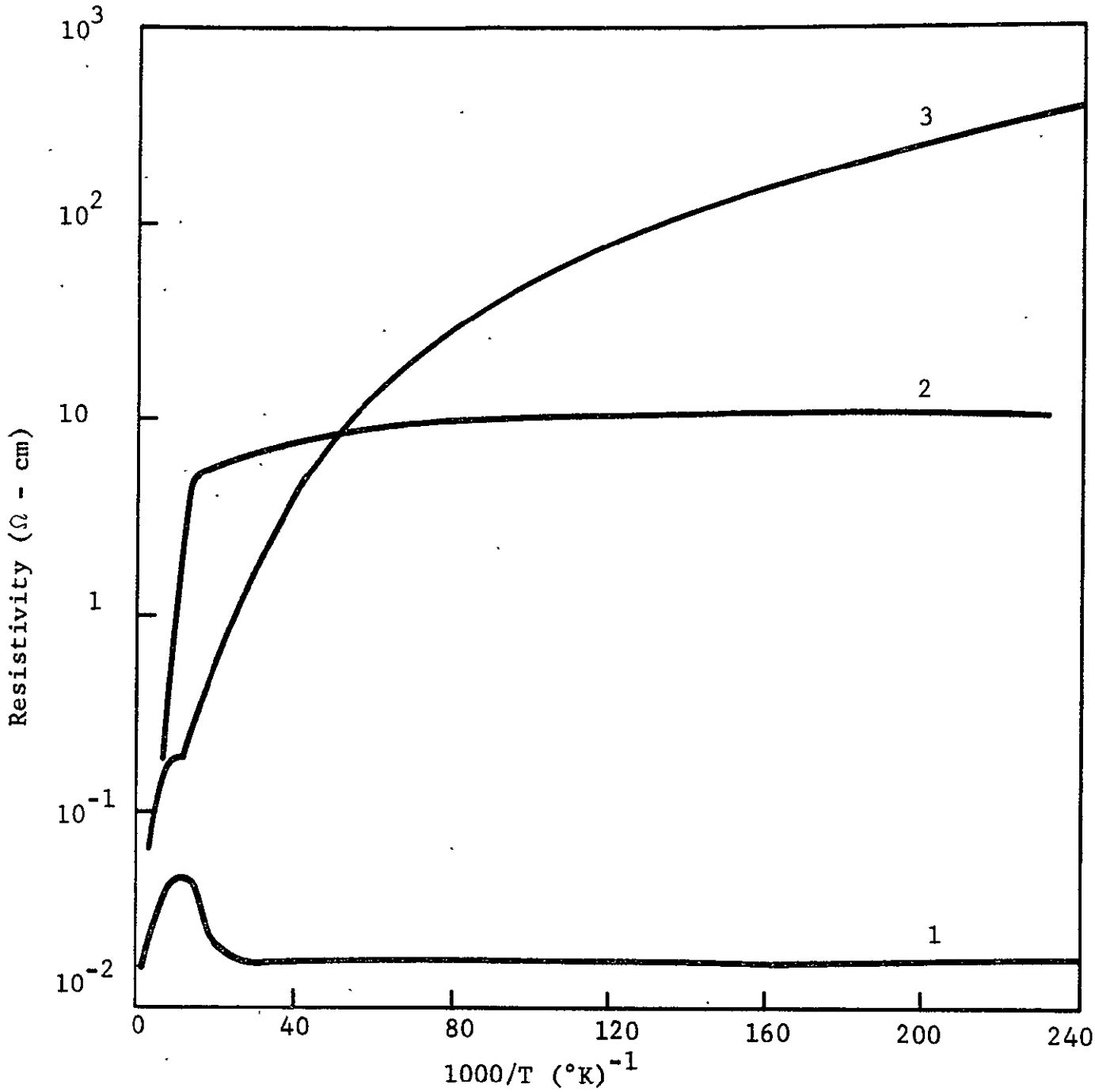

Figure 23 ANOMALOUS BEHAVIOR OF ρ AS FUNCTIONS OF TEMPERATURE

Data is presented for the $Hg_{1-x}Cd_xTe$ ingot grown for this program. The evaluation data for the crystal is summarized in Table VIII, which gives the peak wavelength of the sample at 77 °K (λp 77 °K), the cutoff wavelength at 95 °K (λ_{co} 95 °K) and the donor concentration, Hall mobility μH, and the resistivity at 77 °K. The material was n-type according to both thermal probing and the Hall measurements. The low mobility values suggest that the material may be partially compensated. The Hall coefficient and resistivity versus temperature is shown in Figure 24 for Sample 188/F3. The material is anomalous to type 2. This explains why the 1/f noise coefficient is fairly high.

2.2.8 Analysis of Two-Color Detector Performance

The computer program for the complete prediction of photodetector properties has been extended to include two-color (Hg,Cd)Te photoconductive detector performance. The total program is shown in the flow diagram in Figure 25. The factors included in calculating the performance of the bottom detector of a two-color sandwich include the reflection losses at all the interfaces and the absorption losses as a function of wavelength of the top detector (Hg,Cd)Te and the epoxy separating the top and bottom detectors. The absorption data for (Hg,Cd)Te is based on the work of M.W. Scott of the Honeywell Corporate Research Center (J. Appl. Phys. 40, 4077, 1969).

The calculated responsivity of a two-color (Hg,Cd)Te detector is shown in Figure 26. The cut-off wavelength of the top detector is 9.5 μm and the cutoff wavelength of the bottom detector is 11.6 μm. The rejection ratio, given by responsivity of the bottom detector at the peak (10.8 μm) divided by the responsivity at the trough (9.8 μm) is approximately 1.5. This value is too low, as compared to values observed experimentally. Higher values (~8) have been achieved experimentally. Increased rejection ratios are due to a thicker epoxy layer and absorption band of the epoxy at 9.6 μm. However, too thick an epoxy layer causes reduced transmission in the 10-11 μm region. A major use of the two-color detector computer program has been for the optimization of the detectors, especially with regard to maximizing the rejection ratio. Important variables are the epoxy thickness and absorption coefficient as a function of thickness.

Table VIII

SUMMARY OF EVALUATION OF 10970

Sample No.	λp(77°K) microns	λ_{co}(95°K) microns	N_D cm^{-3}	μ_H $cm^2 V^{-1} s^{-1}$	c(ohm cm)$^{-1}$
128.5/F2	-	-	3.5×10^{15}	5.72×10^{5}	3×10^{-3}
148/F2	8.3	9.0	7.2×10^{14}	3.8×10^{2}	2.24×10^{1}
148/F3	11.0	11.7	5.45×10^{14}	8.87×10^{2}	1.29×10^{1}
163/F2	8.1	8.8	2.67×10^{14}	2.13×10^{3}	1.1×10^{0}
163/F3	10.1	10.8	6.4×10^{14}	1.4×10^{3}	6.87×10^{0}
163/F4	17.0	17.5	7.1×10^{14}	1.6×10^{5}	5.4×10^{-2}
192/F2	9.9	10.7	2.96×10^{14}	4.56×10^{3}	4.64×10^{0}
192/F3	12.3	13.0	5.61×10^{14}	5.55×10^{3}	2.18×10^{0}
192/F4	13.7	14.4	4.66×10^{14}	2.3×10^{4}	5.84×10^{-1}

All material was n-type according to both Hall data and thermal probe measurement.

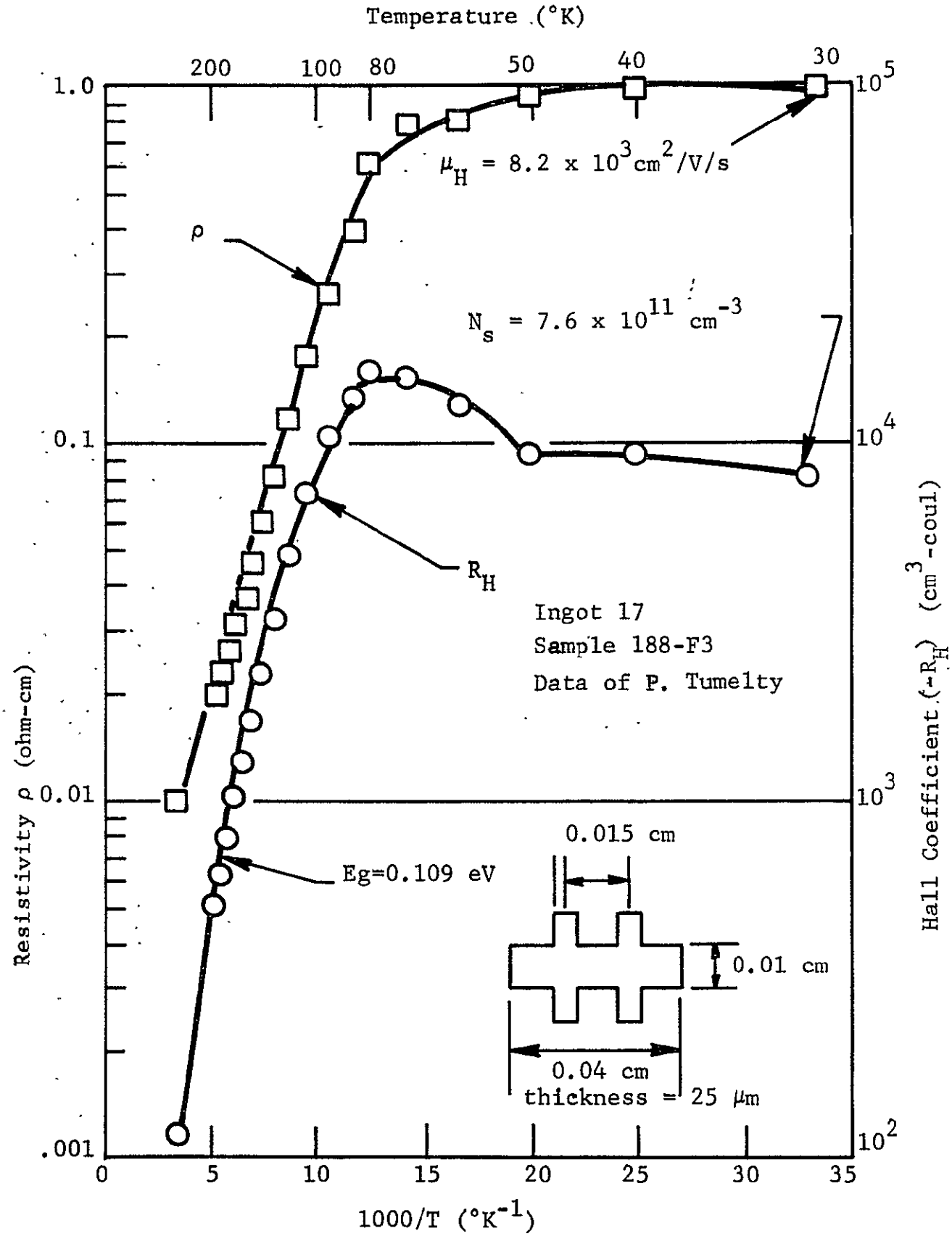
Temperature (°K)
200
100
80
50
40
30
1.0
0.1
0.01
.001
10^5
10^4
10^3
10^2
$\mu_H = 8.2 \times 10^3 cm^2/V/s$
ρ
$N_s = 7.6 \times 10^{11} cm^{-3}$
R_H
Ingot 17
Sample 188-F3
Data of P. Tumelty
Eg=0.109 eV
0.015 cm
0.01 cm
0.04 cm
thickness = 25 μm
Resistivity ρ (ohm-cm)
Hall Coefficient ($-R_H$) (cm^3-coul)
0
5
10
15
20
25
30
35
1000/T ($°K^{-1}$)

Figure 24

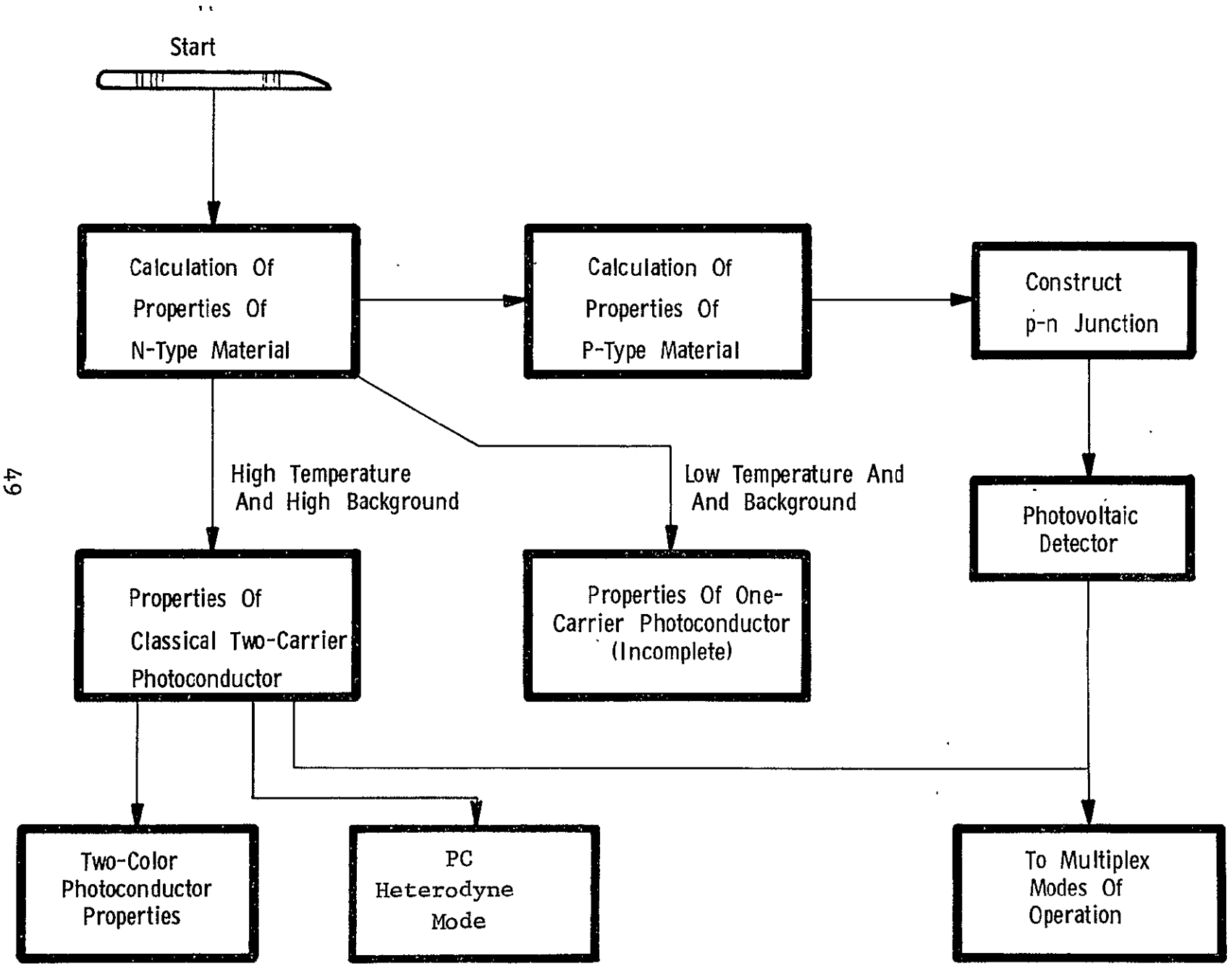

Figure 25 FLOW DIAGRAM - COMPLETE PREDICTION OF PHOTODETECTOR PROPERTIES IN $Hg_{1-x}Cd_xTe$

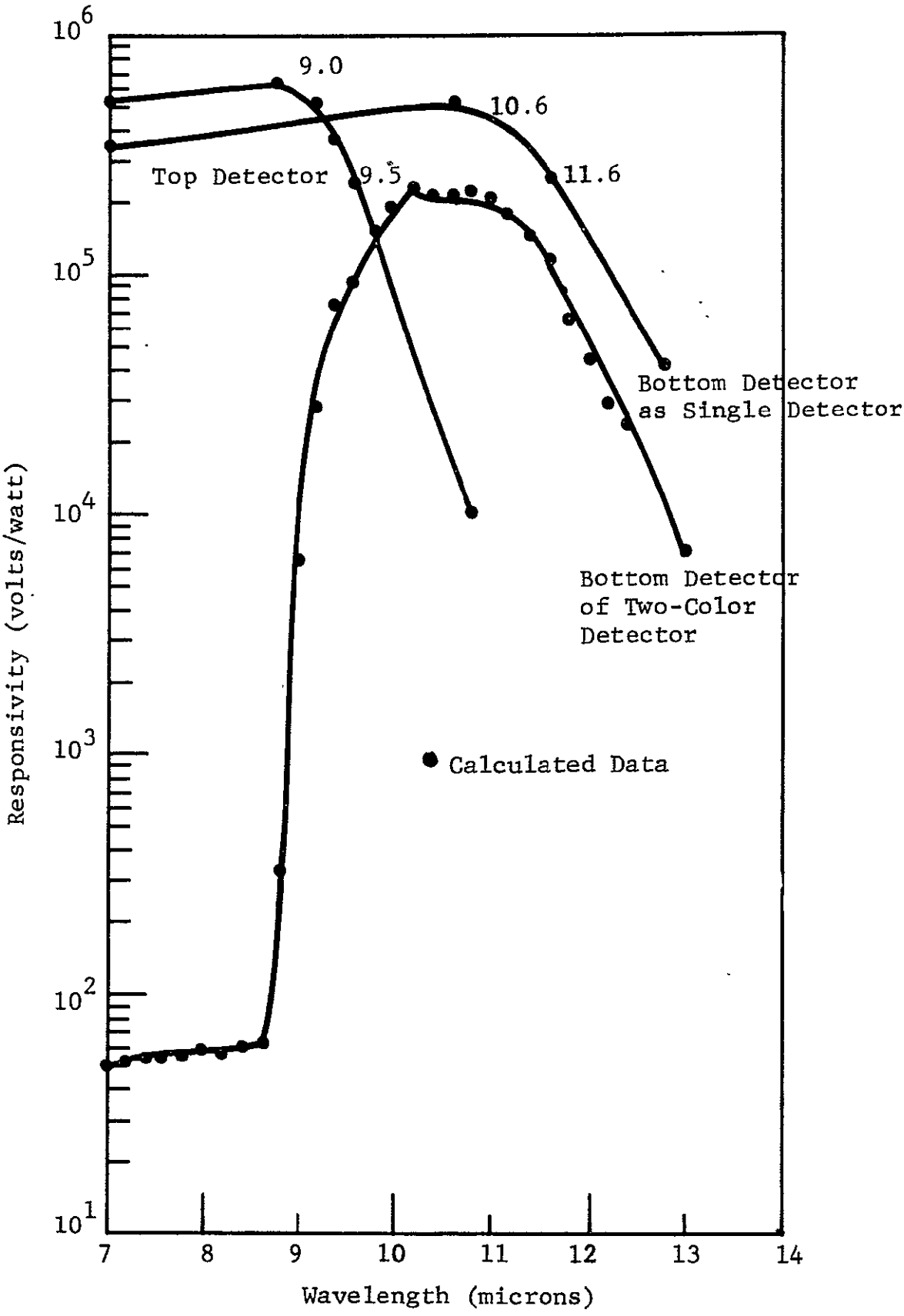

Figure 26 CALCULATED RESPONSIVITY OF TWO-COLOR (Hg,Cd)Te PHOTOCONDUCTOR INCLUDING ABSORPTION OF EPOXY

SECTION III

PERFORMANCE OF THE TWO-COLOR DETECTORS DELIVERED TO NASA/GSFC

Two two-color detectors were delivered to NASA/GSFC under this contract. The data for these detectors is given in Table IX.

The detectors are mounted in a vehicle which is designed for mounting on the cold finger of a variable temperature dewar. The vehicle contains an Irtran II window internally and an externally mounted filter made on a Ge substrate. The vehicle was mounted in a variable temperature dewar with a second Irtran II window. Thus, the detectivity was measured with the detector viewing through two Irtran windows and a Ge window. Properly, only one window should be used and in actual use, only one window, the Ge filter, would be used. Applying the correction factor of 1.3 per window, the recorded D^*_λ's should be multiplied by $(1.3)^2$.

TABLE IX

PERFORMANCE DATA OF TWO-COLOR DETECTORS

1.0	Description	
1.1	Identification Number	DLK96A1 S/N Y1
1.2	HRC Number	21068S 145/182 No. 2
1.3	Detector Type	Photoconductive
1.4	Date of Manufacture	July, 1971
1.5	Window	Ietran II
1.6	Element Size Top Detector	Length 0.254 mm Width 0.0254 mm
1.7	Element Size Bottom Detector	Length 0.0254 mm Width 0.0254 mm
1.8	Element to Well Top	0.1578 Inch
2.0	Test Results Top Detector at 95 °K	
2.1	Resistance	278 Ohms
2.2	Detector Time Constant	Less than 1 μs
2.3	Optimum Bias	0.7 mA
2.4	Peak Spectral Response	8.5 μm
2.5	D^*_{bb} (500, 10 kHz, 1)	2.19×10^8 cm-Hz$^{1/2}$W^{-1}
2.6	D^*_{λ} (8.5 μm, 10 kHz, 1)	3.52×10^9 cm-Hz$^{1/2}$W^{-1}
3.0	Test Results Bottom Detector at 95 °K	
3.1	Resistance	266 Ohms
3.2	Detector Time Constant	Less than 1 μs
3.3	Optimum Bias	0.9 mA
3.4	Peak Spectral Response	10.5 μm
3.5	D^*_{bb} (500, 10 kHz, 1)	4.15×10^8 cm-Hz$^{1/2}$W^{-1}
3.6	D^*_{λ} (10.5 μm, 10 kHz, 1)	9.58×10^9 cm-Hz$^{1/2}$W^{-1}

NOTE: All D* readings were made in a vehicle through an Irtran window. The intrinsic detectivity is therefore 1.3 times the recorded detectivities listed in this report.

2.6 D* vs Bias

TOP ELEMENT

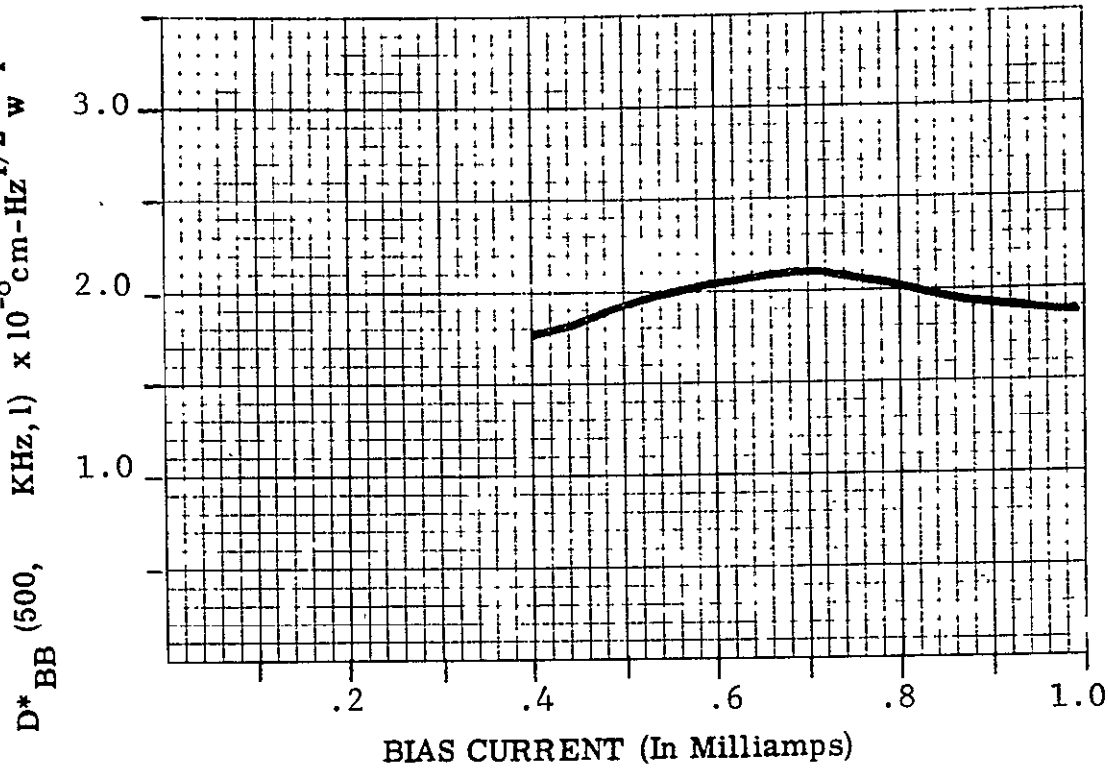

2.5 Relative Spectral Response

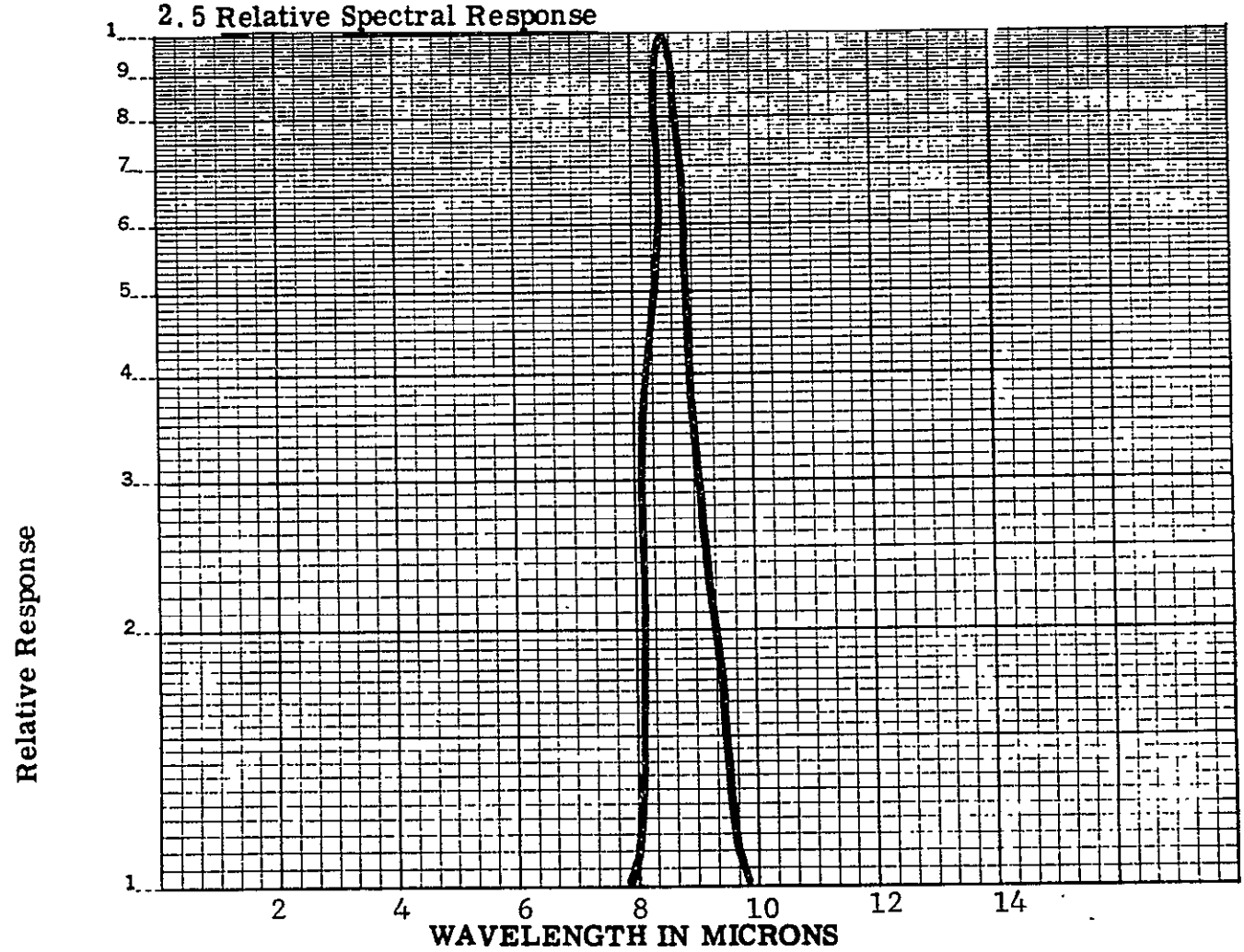

SECTION 2. GRAPHS DLK 96A1 S/N Y1

2.6 D* vs Bias

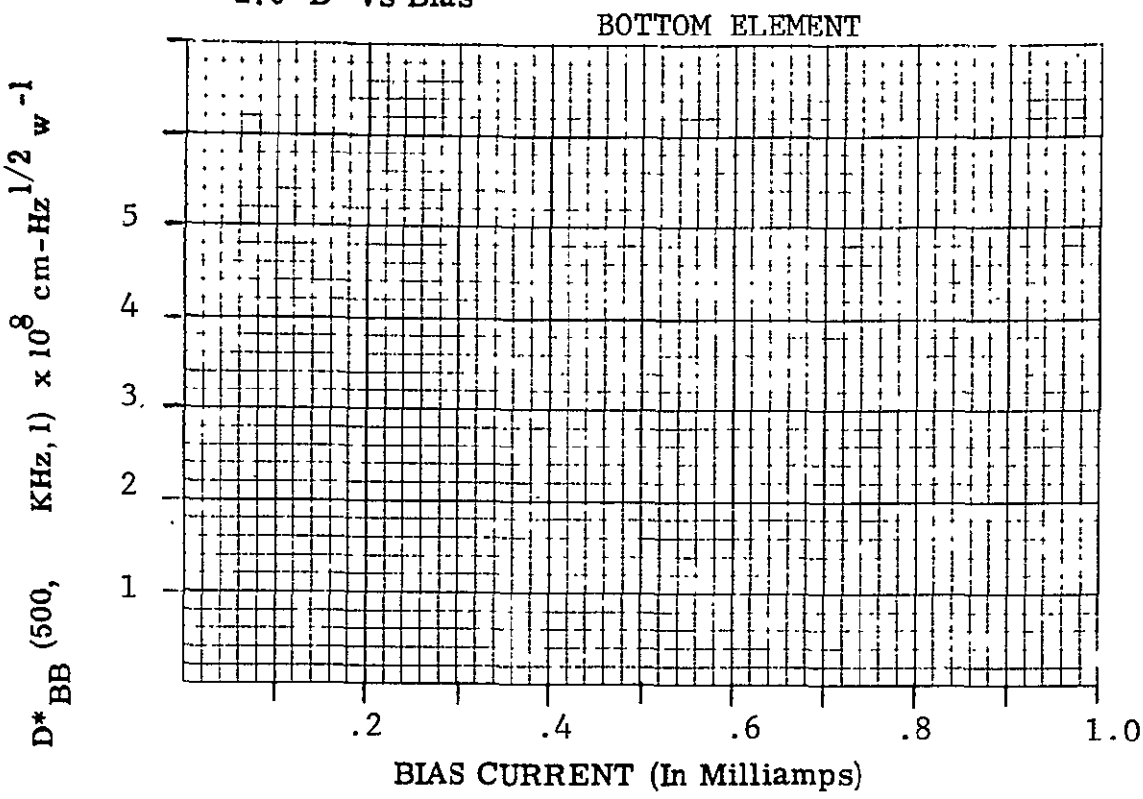

2.5 Relative Spectral Response

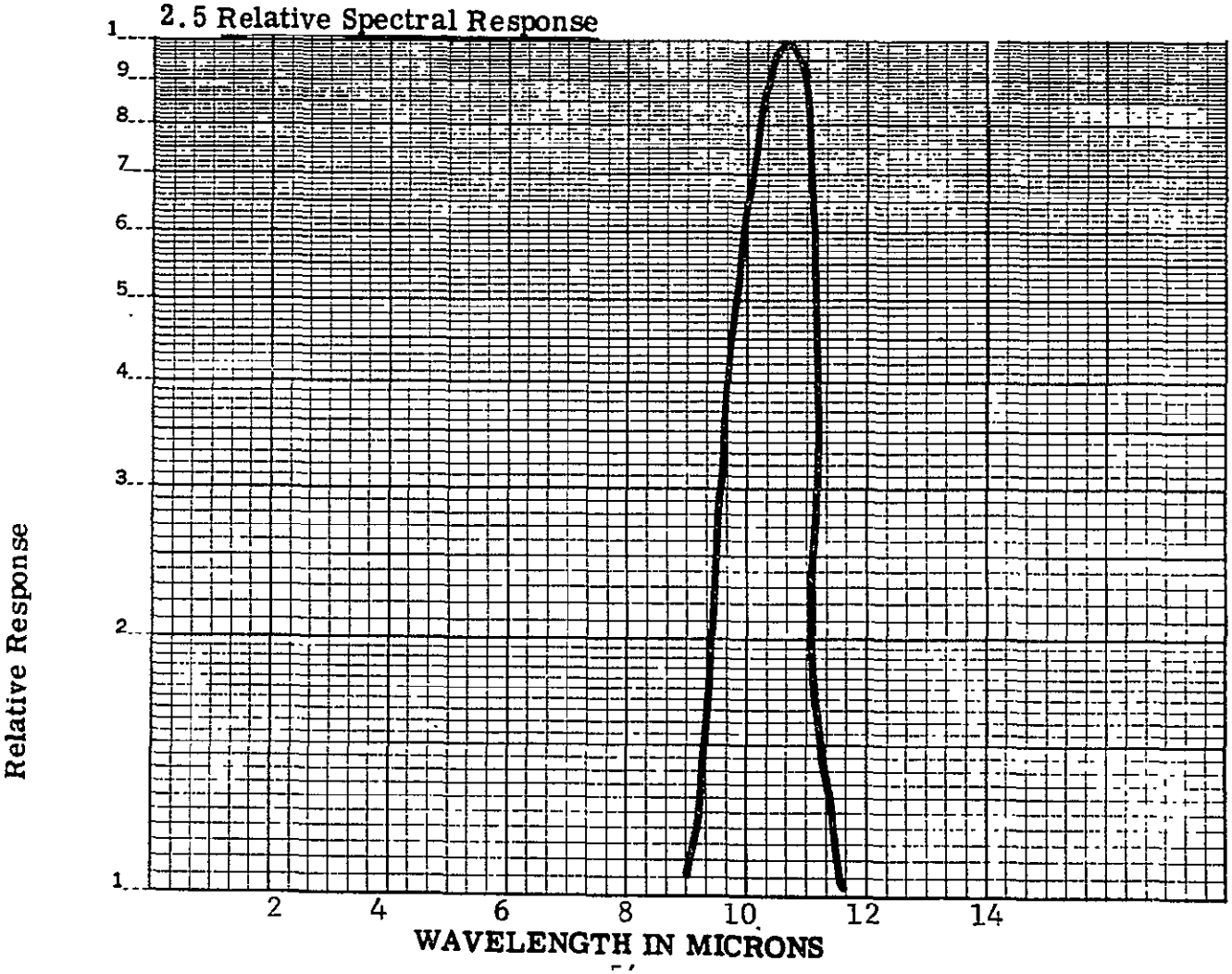

1.0 Description of Detector

1.1	Identification Number	DLK96A1 S/N Y2
1.2	HRC Number	21068S 145/182 No. 5
1.3	Detector Type	Photoconductive
1.4	Date of Manufacture	July, 1971
1.5	Window	Irtran II
1.6	Element Size Top Detector	Length 0.254 mm Width 0.254 mm
1.7	Element Size Bottom Detector	Length 0.254 mm Width 0.254 mm
1.8	Element to Well Top	0.1585 Inch

2.0 Test Results Top Element at 95 °C

2.1	Resistance at 77 °K	1030 Ohms
2.2	Detector Time Constant	Less than 1 μs
2.3	Optimum Bias	0.1 mA
2.4	Peak Spectral Response	9 μm
2.5	D^*_{bb} (500, 10 kHz, 1)	4.5×10^8 cm-Hz$^{1/2}$W^{-1}
2.6	D^*_{λ} (9 μm, 10 kHz, 1)	4.84×10^9 cm-Hz$^{1/2}$W^{-1}

3.0 Test Results Bottom Element at 95 °C

3.1	Resistance at 77 °K	220 Ohms
3.2	Detector Time Constant	Less than 1 μs
3.3	Optimum Bias	1.0 mA
3.4	Peak Spectral Response	10.5 μm
3.5	D^*_{bb} (500, 10 kHz, 1)	1.27×10^8 cm-Hz$^{1/2}$W^{-1}
3.6	D^*_{λ} (10.5 μm, 10 kHz, 1)	1.12×10^9 cm-Hz$^{1/2}$W^{-1}

2.6 D* vs Bias

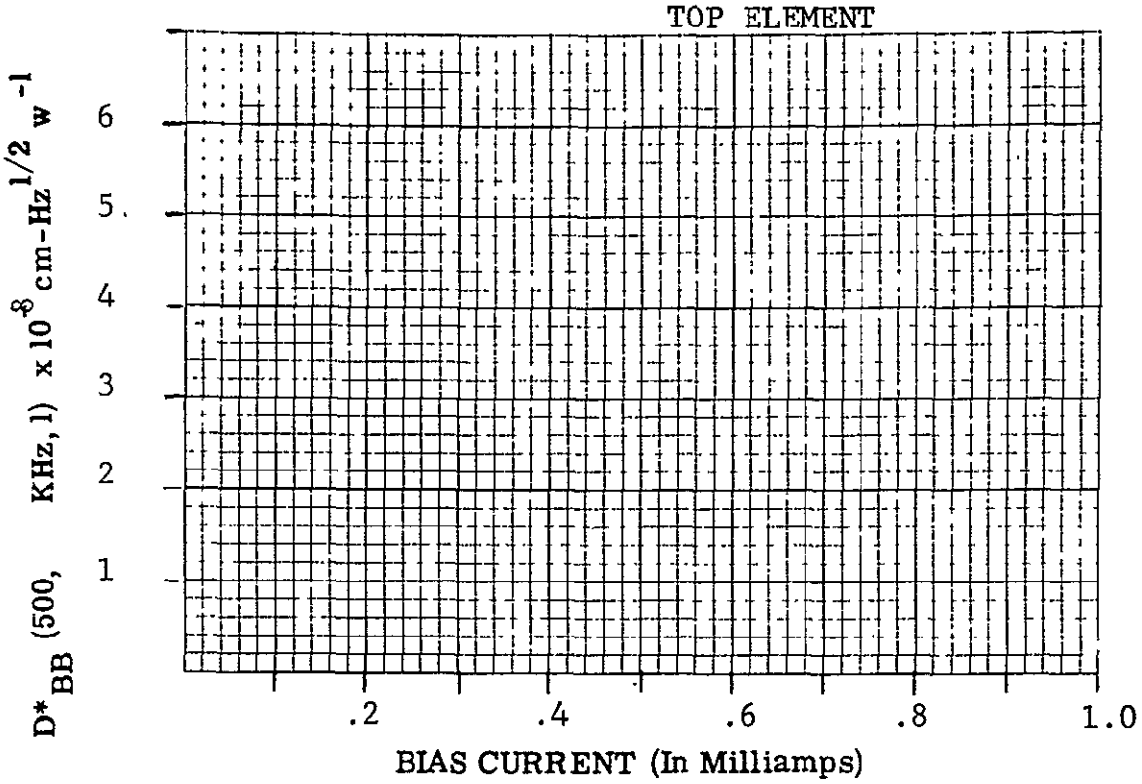

2.5 Relative Spectral Response

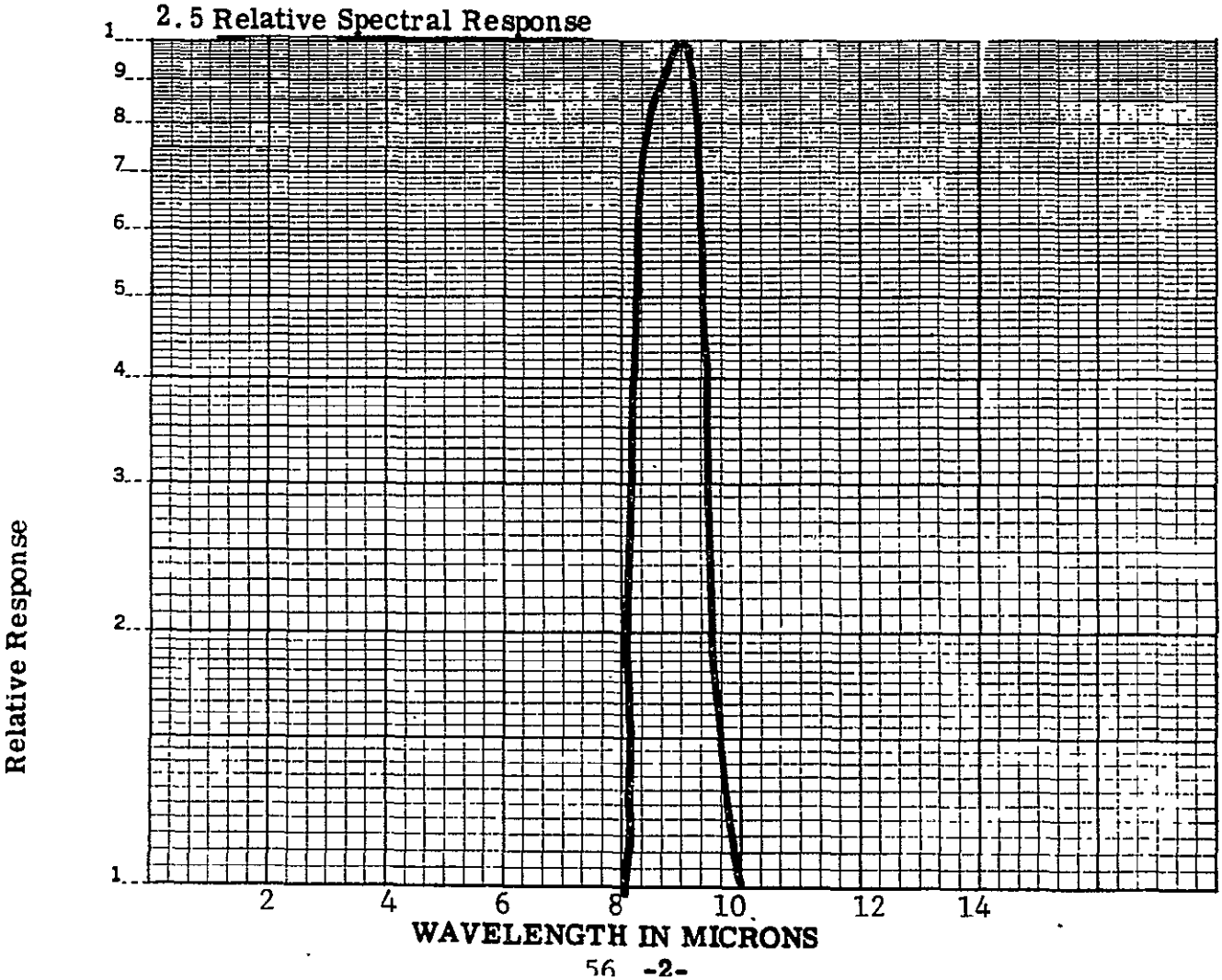

2.6 D* vs Bias

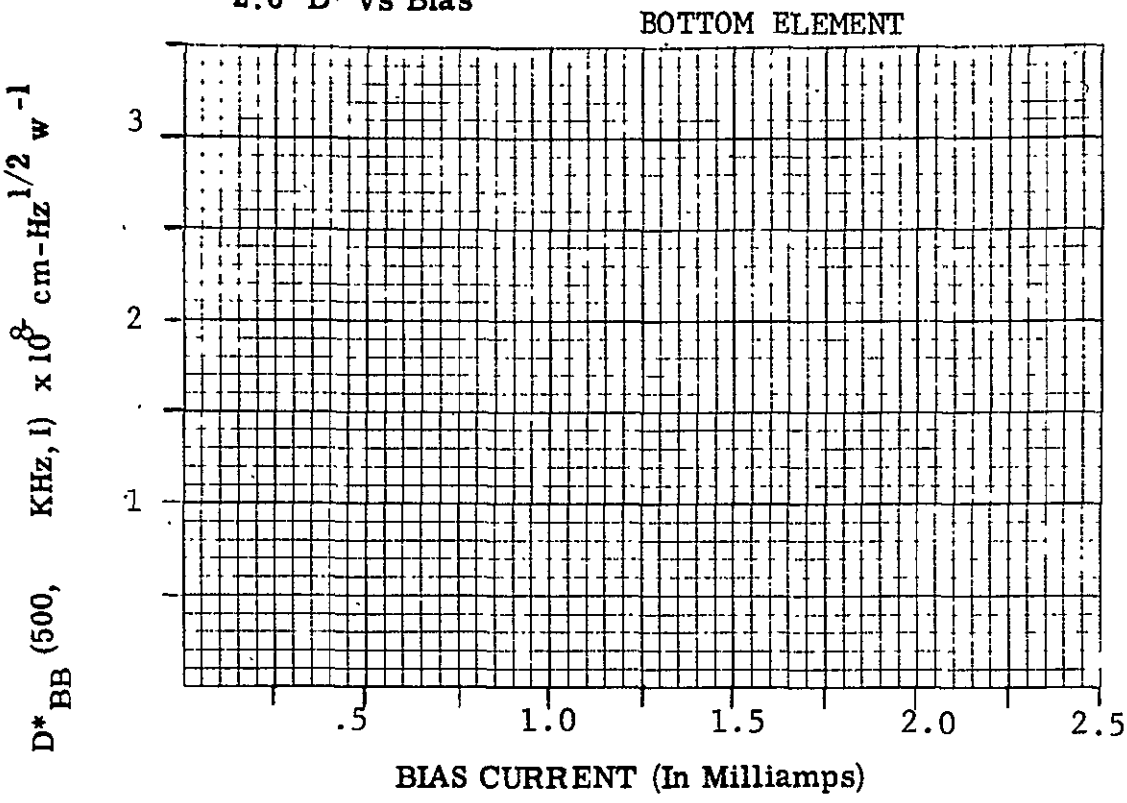

2.5 Relative Spectral Response

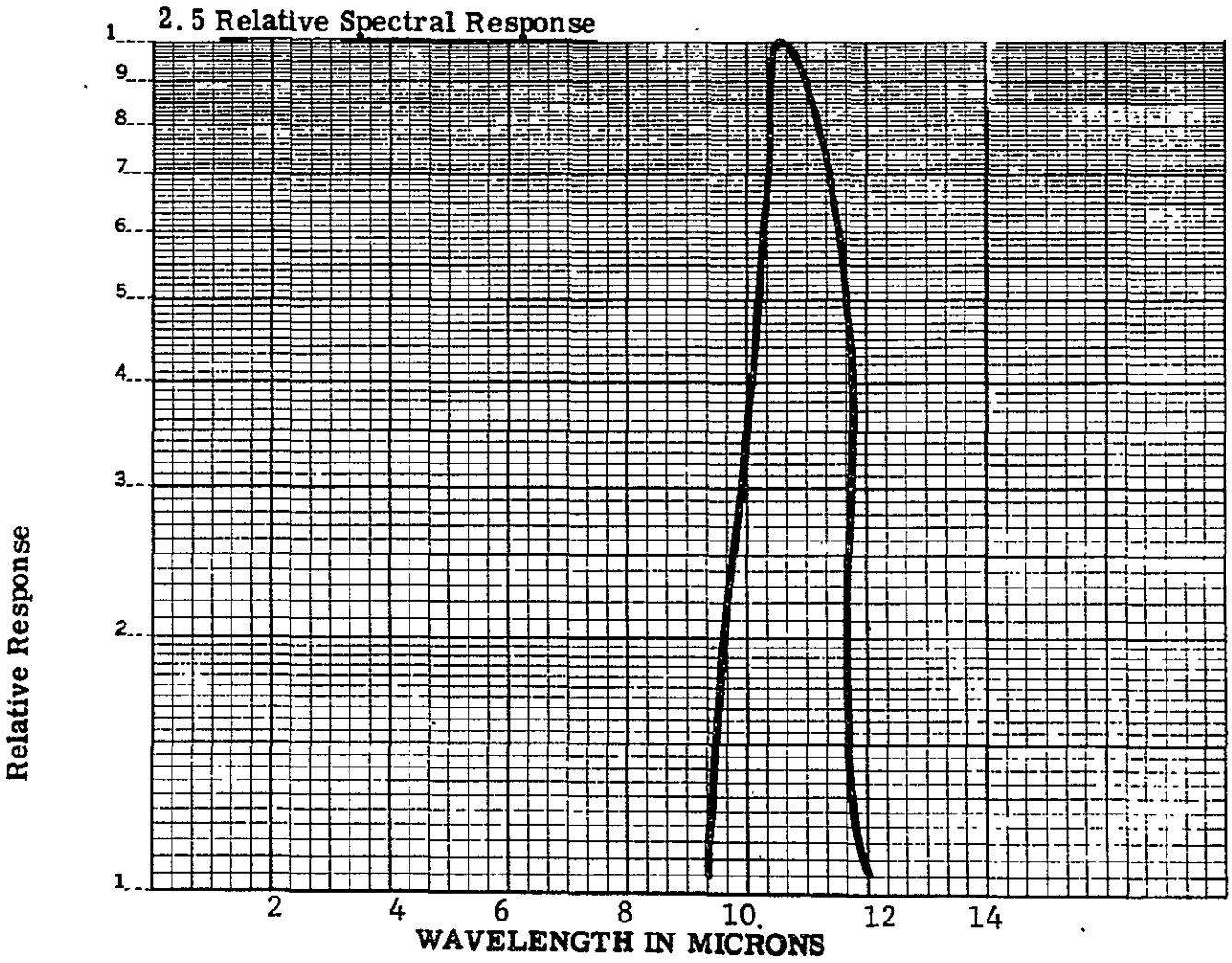

SECTION IV

RECOMMENDATIONS

Based upon the experimental and analytical results of this contract, optimization of two-color (Hg,Cd)Te photoconductive detectors should be continued.

Emphasis should be placed upon developing (1) more refined processing techniques, (2) more advanced spectral data, and (3) more extensive electrical characterization, so that the final devices delivered under future programs will have (1) higher performance, (2) higher spectral resolution, (3) a higher rejection ratio, and (4) a greater versatility for the selection of the spectral channels desired.

During the present two-color detector program processing techniques were developed for making two-color photoconductive detectors with low electrical crosstalk, low optical crosstalk (leakage), good resolution, rejection of the ozone emission band at 9.6 μm, and medium level performance.

The areas of study for future programs should include the following:

1. Radiation Losses:

   (a) Anti-reflection coating of all (Hg,Cd)Te surfaces.
   (b) Improved structural design

2. 1/f noise characterization of two-color detectors

   (a) Continue to ascertain whether there is excessive 1/f noise in two-color detectors and to seek to correct this defect if it occurs.

3. Resolution studies:

   (a) Maximize rejection ratio

   (b) Comparison of molecular absorption versus band edge absorption of a solid using (Hg,Cd)Te as second layer of two-color three-layer detector.

4. Processing techniques

   (a) Increasing Yields

      1. Use of optical absorption for material preselection.

      2. Use of spectral response for top-element material preselection.

      3. Making plank cuts in $Hg_{1-x}Cd_xTe$ ingot

   (b) Develop new epoxies for additional rejection levels.

5. Advanced analysis

To achieve the highest performance of a two-color detector, the radiation losses to the bottom detector must be minimized. For a background limited detector, the degradation of detectivity of the bottom detector goes as the square root of the radiation loss factor; so the loss must be minimized. Emphasis should be on antireflection coating of $Hg_{1-x}Cd_xTe$ surfaces and on advancing the detector configuration.

Because 1/f noise is a cause of performance degradation in $Hg_{1-x}Cd_xTe$ photoconductors, considerable effort should be made to ascertain that two-color detectors do not contain excessive 1/f noise as compared to conventional (Hg,Cd)Te detectors and to transfer new technology from other 1/f noise programs to the two-color detector program.

Resolution studies should be a major segment of the next program. When a rejection band is to occur (say due to ozone emission) it is not clear whether higher resolution will result from the use of absorption in organic molocules due to bending or stretching of chemical bonds or from the band edge absorption of $Hg_{1-x}Cd_xTe$ used as the second layer of a three-layer, two-color detector.

Processing studies must be continued from the perspective of increasing yields and performance. Spectral response data has been used to locate prime areas for the top detectors. The effort should be extended to include optical absorption data. It is believed that this procedure has the advantage that constant composition lines in the material can be determined prior to any

cutting of the slab or plank. Plank cuts are currently being used to increase the amount of material of the desired cutoff wavelength.

Finally, analysis should be continued to maximize the current programs achievements and provide a basis for future work.

APPENDIX A

THE TRANSMISSION THROUGH A MEDIUM SURROUNDED BY TWO DIFFERENT MEDIA

The derivation of the transmission through a medium surrounded by two different media is similar to the case of a media surrounded by the same medium(see Appendix A - First Quarterly Report) except that the front and back surface reflectance is different. If P_i is the incident radiation power on the material as seen in Figure A.1, the power transmitted through to the third medium is equal to:

$$P_t = P_{t1} + P_{t2} + P_{t3} + \ldots P_{tn} + \ldots$$

$$= P_i [(1-\rho_{12})(1-\rho_{23}) \exp(-\alpha d) + (1-\rho_{12})\rho_{23}(1-\rho_{23})$$

$$\exp(-3\alpha d) + (1-\rho_{12})\rho_{23}^2 \rho_{12}^2 (1-\rho_{23}) \exp(-5\alpha d)$$

$$+ (1-\rho_{12}) \rho_{23}^3 \rho_{12}^3 (1-\rho_{23}) \exp(-7\alpha d) + \ldots\ldots]$$

where

$$\rho_{12} = \left(\frac{\eta_1-\eta_2}{\eta_1+\eta_2}\right)^2 \quad \text{and} \quad \rho_{23} = \left(\frac{\eta_2-\eta_3}{\eta_2+\eta_3}\right)^2$$

d = the thickness of the intermediate medium

α = the absorption coefficient of the medium

η_1 = the index of refraction of the initial medium

η_2 = the index of refraction of the intermediate medium

η_3 = the index of refraction of the final medium

Factoring out common factors yields:

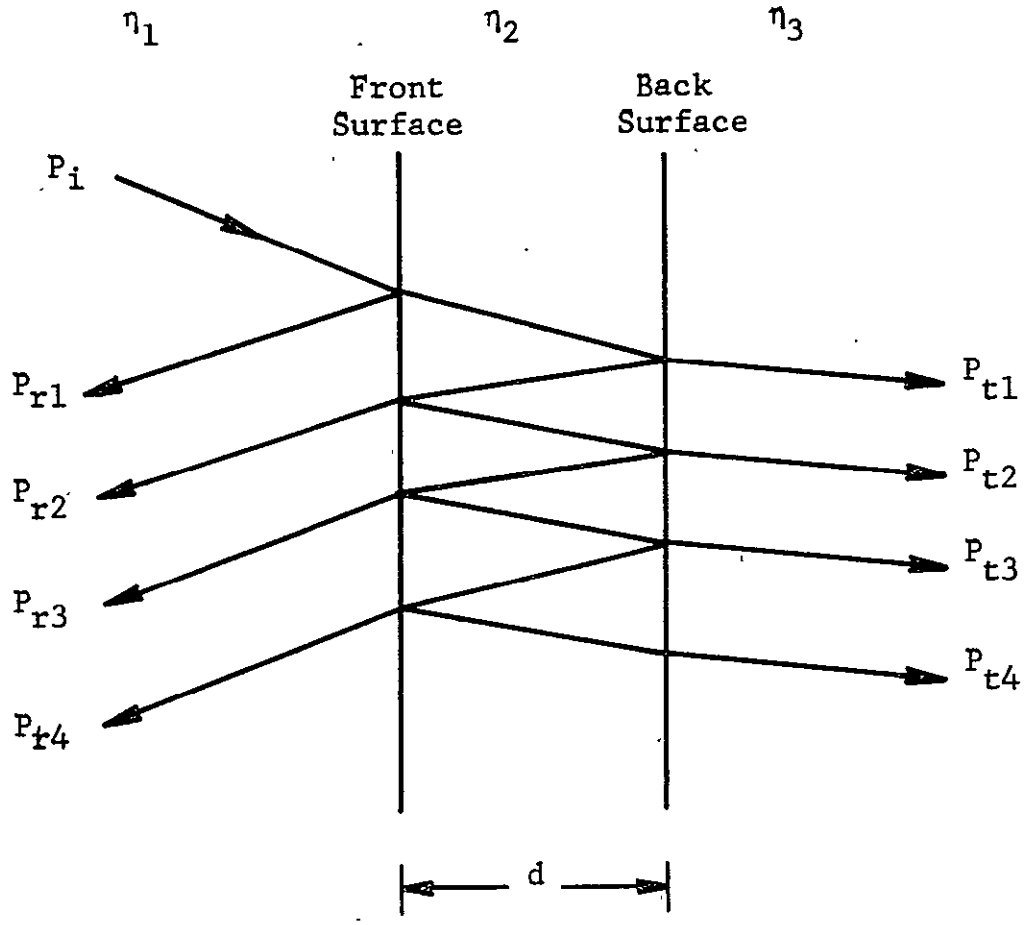
η_1
η_2
η_3
Front Surface
Back Surface
P_i
P_{r1}
P_{r2}
P_{r3}
P_{t4}
P_{t1}
P_{t2}
P_{t3}
P_{t4}
d

Figure A1

$$P_t = P_i \left[(1-\rho_{12})\ (1-\rho_{23})\ \exp\ (-\alpha d)\right] \left[1+\rho_{12}\rho_{23}\ \exp\ (-2\alpha d)\right.$$

$$\left. + \rho_{23}^{2}\ \rho_{12}^{2}\ \exp\ (-4\alpha d) + \rho_{23}^{3}\ \rho_{12}^{3}\ \exp\ (-6\alpha d) + \ldots\right]$$

Since the final factor constitutes a geometrical series the power transmitted P_t is equal to:

$$P_t = P_i \frac{\left[(1-\rho_{12})\ (1-\rho_{23})\ \exp\ (-\alpha d)\right]}{1-\rho_{12}\rho_{23}\ \exp\ (-2\alpha d)}$$

Since $1-\rho_{12} = \tau_{12}$ and $1-\rho_{23} = \tau_{23}$ where $\tau_{12} = \frac{4\ \eta_1\eta_2}{(\eta_1+\eta_2)^2}$

is the transmissivity at the front surface and

$\tau_{23} = \frac{4\eta_2\eta_3}{(\eta_2+\eta_3)^2}$ is the transmissivity at the back

surface, the power transmitted P_t is equal to:

$$P_t = P_i \frac{\left[\tau_{12}\tau_{23}\ \exp\ (-\alpha d)\right]}{1-\rho_{12}\rho_{23}\ \exp\ (-2\alpha d)}$$

and the transmittance $\tau = \frac{P_t}{P_i} = \frac{\tau_{12}\tau_{23}\ \exp\ (-\alpha d)}{1-\rho_{12}\rho_{23}\ \exp\ (-2\alpha d)}$

APPENDIX B

EFFECTIVE QUANTUM EFFICIENCY OF THE BOTTOM DETECTOR - PARALLEL CONFIGURATION (NO TOP SUBSTRATE)

A simple effective quantum efficiency for the bottom detector in the parallel configuration with no top substrate can be readily derived using Figure B.1. If P_{it} is the incident power on a two color detector, the power incident upon the bottom detector P_{ib} is equal to

$$P_{ib} = P_t \cdot A_e$$

where $P_t = \frac{P_{it} [\tau_{12}\tau_{23} \exp(-\alpha_T d_T)]}{1-\rho_{12}\rho_{23} \exp(-2\alpha_T d_T)} = P_{it} \tau_t$

is the power transmitted through the top detector and A_e is the percent absorbed by the interface epoxy layer. τ_{12}, τ_{23}, ρ_{12}, and ρ_{23} are as given in Appendix A while d_T is the thickness of the top detector and α_T is the absorption coefficient of the top detector at the wavelength of interest. Since this model assumes minimal multiple reflections in the interface layer, the power absorbed in the bottom detector $P_{ab} = \eta_b P_{ib}$ where η_b is the quantum efficiency of the bottom detector between two epoxy layers and is equal to:

$$\eta_B = \frac{(1-\rho_B)[1-\exp(-\alpha_B d_B)]}{1-\rho_B \exp(-\alpha_B d_B)}$$

$\rho_B = \left(\frac{\eta_4-\eta_3}{\eta_4+\eta_3}\right)^2$, d_B is the thickness of the bottom detector and α_B is its absorption coefficient. The final power absorbed by the bottom detector is equal to:

$$P_{ab} = \eta_b P_t A_e = \eta_b A_e \tau_t P_{it}$$

Therefore in terms of the incident radiation P_{it}, the effective quantum efficiency of the bottom detector is equal to:

$$\text{Effective Quantum Efficiency} = \eta_b \, A_e \, \tau_t$$

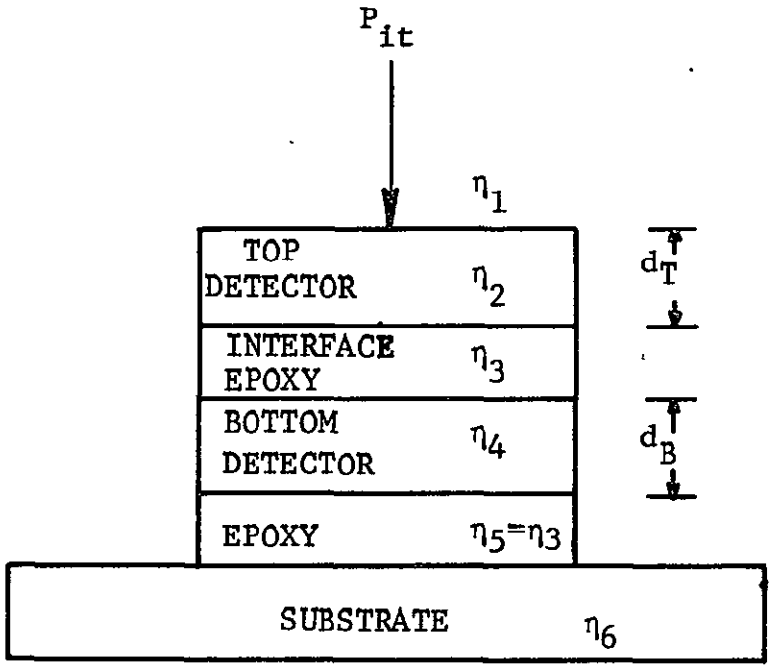

Figure B1